Main revisions and response to reviewers' comments

Manuscript No.: acp-2020-176

Title: Characterization and source apportionment of aerosol light scattering in a typical polluted city in Yangtze River Delta, China

Authors: Dong Chen, Yu Zhao, Jie Zhang, Huan Yu, Xingna Yu

We thank very much for the valuable comments and suggestions from the two reviewers, which help us improve our manuscript significantly. The comments were carefully considered and revisions have been made in response to suggestions. Following is our point-by-point responses to the comments and corresponding revisions.

Reviewer #1

0. The paper by Chen et al. systematically investigates the characteristics and sources of aerosol light scattering through measurements at three different functional sites in a typical polluted city in the Yangtze River Delta, China. Aerosol scattering is important for both visibility degradation and air pollution, and is also complex due to aerosol chemical composition and hygroscopic growth. In this study, the US IMPROVE formula for aerosol scattering calculation was optimized using online and offline measurements at different functional sites in Nanjing with complicated sources of air pollutants. The influence of aerosol size distributions and pollution levels on the aerosol scattering was quantitatively evaluated based on a comprehensive analysis of the size-specific chemical compositions of particles at various sites. In general, this manuscript is well organized and easy to follow. I would recommend its acceptance after some necessary corrections suggested as follows:

Response and revisions:

We appreciate the reviewer's positive remarks on the importance of the work.

1. Line 87: "NH_4NO_3 and $(NH_4)_2SO_4$" need to be defined at their first mention in the

manuscript. The manuscript has similar problems with other chemical species as well. Please go through the manuscript and change all of them.

Response and revisions:

We thank the reviewer's reminder. As suggested, the two species were defined at their first appearance (**lines 88 in the revised manuscript**). We have also checked through the manuscript and revised all other items that need to be defined.

2. Line 149: What is the mass fraction of the methanol soluble organic carbon in the total organic carbon mass? Did you try the water extraction?

Response and revisions:

We thank the reviewer's comment. Figure R1 illustrates the relationship between the total organic carbon (OC) and methanol soluble organic carbon (MSOC) concentrations in this study. The average MSOC was 8.23 ± 4.84 μg/m^3 and accounted for 88% of the total OC mass in all samples. This result was similar to the fraction of 85% estimated by Cheng et al. (2016). Considering that a large fraction of brown carbon (BrC) absorption comes from OC insoluble in water, water extraction (WSOC) method was thus not applied in the current study. We have added the discussion **in lines 174-181 in the revised manuscript**, and provided Figure R1 as **a new Figure S4 in the revised supplement**.

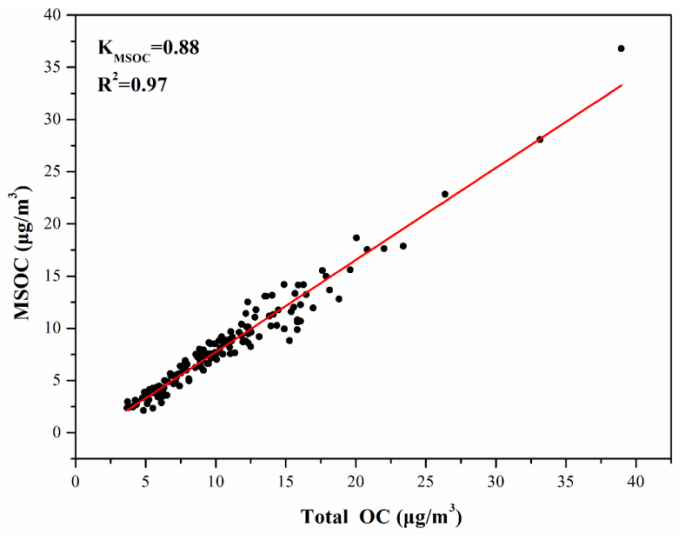

Figure R1. Correlation between MSOC and total OC for all the samples collected in this work. The red line indicates linear regression results with K as slope (intercept is set at zero).

3. Line 186: In the process of formula optimization, why did the authors subtract the scattering coefficients by sea salt, soil dust and coarse particles from the measured scattering coefficient? Does it mean that the light scattering of those species has little impact on the optimization of IMPROVE formula?

Response and revisions:

We thank the reviewer's comment. Figure R2 presents the ratios of the collective scattering coefficients of the sea salt and soil to the total $PM_{2.5}$ scattering at the three sites. The ratios were 0.083, 0.093 and 0.081 at NJU, PAES, and NUIST, respectively, i.e., the scattering coefficients by sea salt and soil dust accounted for less than 10% of the total $PM_{2.5}$ light scattering. Therefore the impact of the two species on the optimization of IMPROVE algorithm should be limited. In order to be concise in the algorithm optimization and to ensure the stability of the multiple linear regression, the independent variables contained $(NH_4)_2SO_4$, NH_4NO_3 and OM in the optimized formula, and the light scattering of sea salt and soil dust was subtracted from the measured scattering coefficient of $PM_{2.5}$. We have clarified the methodology **in lines 217-220 in the revised manuscript**, and have added the discussion **in lines 459-465 in the revised manuscript**. **A new Figure S10** (i.e., Figure R2) has also been provided in the revised supplement.

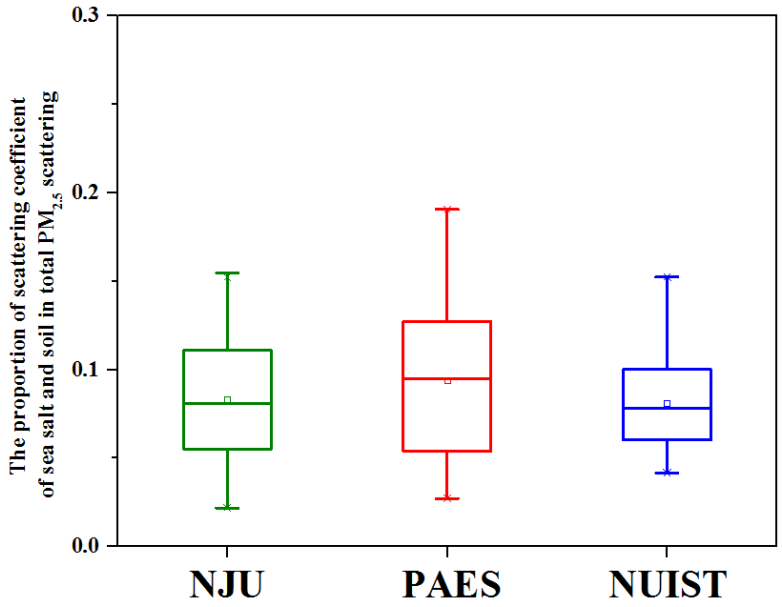

Figure R2 The collective proportions of sea salt and soil dust to the total $PM_{2.5}$ scattering coefficient at the three sites based on the IMPROVE2007 algorithm.

4. Line 201: Mie theory is very sensitive to the size distribution of aerosol chemical species. However, the size distribution data obtained from a high-flow MOUDI impactor can usually be influenced by the particle bounce. This is particularly concerned in case where filters, instead of metal foils with grease coating, are used as the substrate. I suggest the authors make an uncertainty evaluation upon the size distribution measurement in this study.

Response and revisions:

We thank the reviewer's comment. Although application of metal foils with grease coating could avoid the particle bounce, it might change the result of chemical species measurement. More, the metal foils substrate cannot meet the requirement of carbonaceous aerosol analysis, due to its special heating up program. In this study, therefore, we selected teflon filter for ion and element analysis, and quart fiber filter for carbonaceous aerosol analysis. Teflon filter membrane was generally applied for size-resolved particles sampling by MOUDI with excellent results (Contini et al., 2014; Gao et al., 2016; Guo et al., 2010). Taking NJU as an example, excellent agreement was found between the mass concentrations of $PM_{1.8}$ collected with quartz fiber in MOUDI impactor and $PM_{2.5}$ collected with TH-150 samplers, as shown in Figure R3. Therefore, the effect of particle bounce was expected to limited in this study. We have added the information **in lines 157-161 in the revised manuscript**, and provided **a new Figure S3** (Figure R3 here) in the revised supplement.

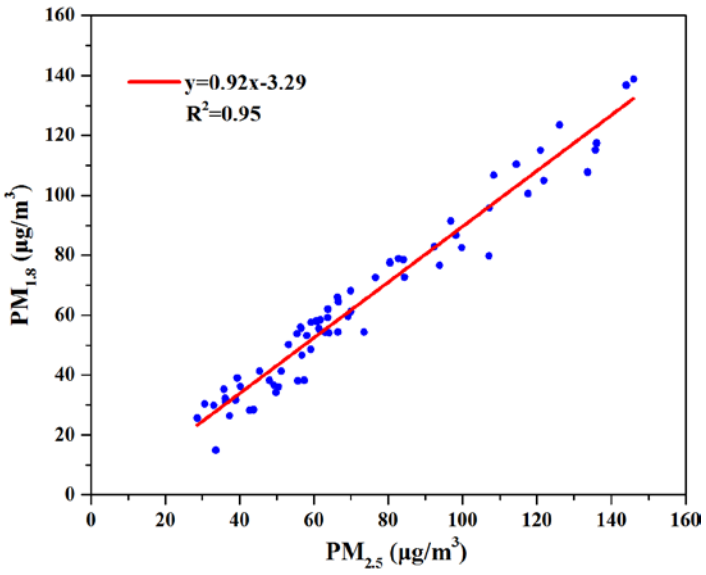

Figure R3 Correlation between the mass concentrations of $PM_{1.8}$ collected with MOUDI impactor and $PM_{2.5}$ collected with TH-150C sampler at NJU.

5. In Section 3.2, the US IMPROVE algorithm was optimized only within one city in the Yangtze River Delta with good performance. How did the authors consider the application of the optimized formula in typical regions such as cities in Beijing-Tianjin-Hebei or Pearl River Delta? Some discussions are recommended here.

Response and revisions:

We thank the reviewer's comment. In this study, the optimized IMPROVE formula was obtained based on the measured ambient concentrations of aerosol chemical species at three different functional sites in Nanjing, a typical polluted city in the Yangtze River Delta. As the chemical composition of aerosol (particularly SNA) was the key factor affecting its light scattering, the optimized IMPROVE formula could be applied in nearby cities with similar composition of aerosols in eastern China including Shanghai and Jinan, as we stated **in lines 465-474 in the revised manuscript.** Moreover, for other regions with rapidly developing economy and fast industrialization in China including Beijing-Tianjin-Hebei or Pearl River Delta regions, the current work provides methodology and data support for the studies of aerosol light scattering in cities with relatively serious particle pollution. Given the fast changes in emission control and aerosol pollution in those regions, more campaigns on aerosol optical and chemical properties are recommended to further evaluate and improve the applicability of the optimized IMPROVE algorithm. We have added the explanation **in lines 474-481 in the revised manuscript**.

6. Line 352: The study did not mention if the scattering coefficients used for the US IMPROVE estimation at the three sites were measured by CAPS or nephelometer? According to Section 2.3, the scattering coefficients at PAES and NUIST were measured by two integrating nephelometers. Need some clarification on this issue.

Response and revisions:

We thank the reviewer's reminder and sorry for the error. The scattering coefficients used for the evaluation and optimization of the IMPROVE algorithm at the three sites were all measured with nephelometers. The relevant texts have been revised **in line 399 in the revised manuscript**.

7. Line 447: Due to the varied chemical properties of particles in different regions, the growth factors of particles (GF) can be different, and it would bring some uncertainty to the calculation of scattering coefficient in Section 3.3. It is recommended to measure and apply the local GF values in this work.

Response and revisions:

We thank and agree the reviewer's comment. Due to the lack of suitable instrument like hygroscopicity tandem differential mobility analyzer (H-TDMA), we did not measure the local GF values directly, and it is a limitation of this study. Instead, we collected the GF data from the existing local studies in Nanjing (Table S1 in the supplement), and applied them in estimation of ambient scattering coefficient by Mie theory. To check the uncertainty of this application, the estimates were compared with those calculated with the scattering hygroscopic growth factor (f(RH)), as shown in Figure S12 in the revised supplement (Figure S8 in the original submission). A good agreement was found between the two methods (R^2=0.95), indicating the limited uncertainty from the GF values applied in this study.

8. In Section 3.4, there was no clear description whether the scattering coefficients were estimated based on the assumption of dry or ambient conditions.

Response and revisions:

We thank the reviewer's reminder. The estimated scattering coefficients in Section 3.4 were based on the assumption of ambient condition. The relevant text has been revised **in line 543 in the revised manuscript**.

9. In Section 3.5, the assumption that the secondary components were proportional to the emissions of their precursors is subject to great uncertainty, as noted by the authors. Please be more specific on how to get better results with improved measurement or modeling methods.

Response and revisions:

We thank the reviewer's comment. As we stated in the manuscript, there was substantial uncertainty in the methodology in which source apportionment of secondary aerosols depends on the magnitudes of precursor emissions. It is a limitation of the present study. To

further improve the source apportionment results, some specific tracers of secondary aerosols like semi volatile and low volatile oxygen-containing organic aerosols can be firstly observed with advanced technology such as aerosol mass spectrometry (AMS), and the observation data can then be combined with receptor models to quantify the source contribution of secondary aerosols. Besides, air quality model that integrates particle source apportionment technology (PSAT) is recommended to be applied to evaluate and confirm the performance of the source apportionment of secondary aerosol with the receptor model. We have added the explanation **in lines 678-685 in the revised manuscript**.

10. Some minor comments:

Line 31: Define “IMPROVE” on first usage.

Response and revisions:

We thank the reviewer’s reminder and the full name has been given in the revised manuscript.

Line 32: "OC" should not be abbreviated when it is mentioned for the first time.

Response and revisions:

We thank the reviewer’s reminder and the full name has been given in the revised manuscript.

Line 160: What is the wavelength of the integrating nephelometer at the three sites used?

Response and revisions:

We thank the reviewer’s reminder. The two nephelometers (Ecotech Pty Ltd, Australia, Model Aurora1000G) at NJU and PAES were operated at the wavelength of 520 nm. The integrating nephelometer (Model 3563, TSI, USA) used at NUIST can measure the light scattering at three visible wavelengths (450, 550 and 700 nm), and the scattering coefficient at the wavelength of 550 nm was adopted in this work. We have added the explanation **in lines 190-193 in the revised manuscript**.

Line 246: The operational symbol was missing in Eq. (3).

Response and revisions:

We thank the reviewer's reminder and it is corrected in the revised manuscript.

Line 522: "Mien theory" should be "Mie theory".

Response and revisions:

We are sorry for this mistake and thanks for the reminder. We have corrected it in the revised manuscript.

Line 562: "PME" should be "PMF".

Response and revisions:

We are sorry for this mistake and thanks for the reminder. We have corrected it in the revised manuscript.

Line 970: SIA in the legend did not exist in Figure 8.

Response and revisions:

We thank the reviewer's reminder and the SIA legend in Figure 8 has been removed.

Reference list: The format of references should be in accordance with the journal requirement.

Response and revisions:

We thank the reviewer's reminder. We have checked the format of references and made it consistent with the journal requirement.

References

Cheng, Y., He, K.B., Du, Z.Y., Engling, G., Liu, J.M., Ma, Y.L., Zheng, M., Weber, R.J.: The characteristics of brown carbon aerosol during winter in Beijing, Atmos. Environ., 127, 355-364, doi:10.1016/j.atmosenv.2015.12.035, 2016.

Contini, D., Cesari, D., Genga, A., Sicilianob, M., Ielpo, P., Guascito, M. R., Conte, M.: Source apportionment of size-segregated atmospheric particles based on the major

water-soluble components in Lecce (Italy), Sci. Total Environ., 472, 248-261, 10.1016/j.scitotenv.2013.10.127, 2014.

Gao, Y., Lee, S. C., Huang, Y., Chow, J. C., Watson, J. G.: Chemical characterization and source apportionment of size-resolved particles in Hong Kong sub-urban area, Atmos. Res., 170, 112-122, 10.1016/j.atmosres.2015.11.015, 2016.

Guo, S., Hu, M., Wang, Z. B., Slanina, J., and Zhao, Y. L.: Size resolved aerosol water-soluble ionic compositions in the summer of Beijing: implication of regional secondary formation, Atmos. Chem. Phys., 10, 947–959, doi:10.5194/acp-10-947-2010, 2010.

Reviewer #2

0. The current manuscript presents a comprehensive study of the influential factors and source apportionment of aerosol light scattering at three sites in Nanjing, representative for suburban (NJU), urban (PAES) and industrial areas (NUIST) respectively. The data obtained in this work show interesting details on the linkage between chemistry composition and light scattering of aerosols, and help better understanding the effects of various sources on visibility degradation at the city scale. Overall I think the work provides reasonable analysis and the paper is clearly written. Before it can be published in Atmospheric Chemistry and Physics, however, I have some concerns that should be further addressed, and minor revisions are accordingly suggested as below.

Response and revisions:

We appreciate the reviewer's positive remarks on the importance of the work.

1. In line 130, QA/QC procedures of aerosol sampling process are missed in this manuscript, which are important for a scientific paper presenting the first-hand data. For example, the MOUDI sampler could be blocked during heavy pollution conditions, and the collected samples might not be evenly distributed. This phenomenon would affect the chemical analysis, particularly for OC and EC (choice of spots). How did the authors treat such kind of problems or estimate the uncertainty from sampling?

Response and revisions:

We thank the reviewer's comment. To prevent the blocking by particles during sampling, the MOUDI samplers were first cleaned using an ultrasonic bath for 30 min before each sampling. In addition, the sampling flow rate was calibrated before each sampling and was also monitored with the flow meter during the whole sampling period. Those quality control measures assured that the MOUDI samplers were not blocked during the sampling period. Even for heavily polluted days with the $PM_{1.8}$ concentration measured at 128 $\mu g \cdot m^{-3}$, the particles sampled by MOUDI were evenly distributed, as shown in Figure R4. We have added the explanation **in lines 138-144 in the revised manuscript**, and added **a new Figure S2** (Figure R4 here) in the revised supplement.

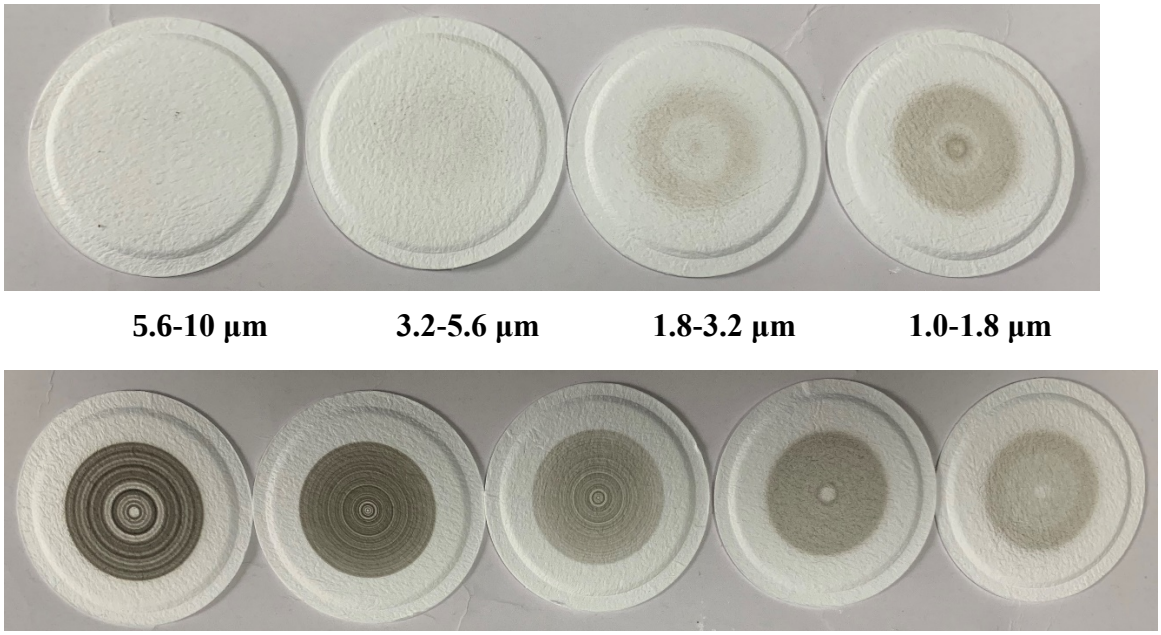

Figure R4 A set of size-resolved particle filter samples on 25 Dec 2015 at NJU. The measured $PM_{1.8}$ and $PM_{2.5}$ were 128 and 141$\mu g/m^3$, respectively.

2. In Line 136, were field blanks obtained during the sampling campaigns? And, why were the sampling periods different at the three sites? Similarly, in Line 128, why was the sampling size at NJU larger than another two sites? The sampling strategy should be described more.

Response and revisions:

We thank the reviewer's comment. Yes we applied field blanks to correct the possible

bias in the analysis of aerosol chemical species. Totally 19 sets of size-segregated blank filters (10, 4 and 5 for NJU, PAES and NUIST, respectively) and 35 daily blank $PM_{2.5}$ filters (25, 6 and 9 for NJU, PAES and NUIST, respectively) were obtained at the three sites. All the blank filters were put in the samplers without inlet air flow for 24 h when the field campaigns finished. We have added the information **in lines 152-157 in the revised manuscript**.

Attributed to weather condition and aerosol sampler maintenance, the sampling periods for the three sites were different. Simultaneous samplings were conducted at the three sites from one week to ten days in each season from summer 2016 to winter 2016-2017. For the remaining time, two MOUDI samplers were applied to collect Teflon and quartz filter samples simultaneously at one of the three sites. As the Cavity Attenuated Phase Shift Albedo monitor (CAPS) was only installed at NJU and large amounts of data on aerosol optical and chemical information were needed to examine the influence of relative humidity on aerosol light scattering (Section 3.3), the sampling size at NJU was larger than another two sites. We have added the explanation **in lines 144-152 in the revised manuscript**.

3. In Line 145, Sunset analyzer was able to measure thermal EC and OC, and optical EC and OC. The author should clarify it carefully in the paper. Why choose them for the analysis?

Response and revisions:

We thank the reviewer's comment. The Sunset analyzer provides both thermal and optical concentrations for carbonaceous aerosols, and thermal EC and OC were used in this study. The instrument estimates the optical EC by measuring the light attenuation (ATN). As ATN was determined not only by EC but also by brown carbon (BrC), the optical method may overestimate the EC and thus underestimate the OC (Cui et al., 2016; Massabò et al., 2016). Therefore, we applied the measured thermal EC and OC in this study. We added the explanation **in lines 169-173 in the revised manuscript**.

4. In Line 183, what software did authors use to run the multiple linear regression? If this model has been developed or used in other studies, the references should be provided.

Response and revisions:

SPSS 16.0 was used to conduct the multiple linear regressions. This information was added **in line 216 in the revised manuscript** and relative references were provided (Cheng et al., 2011; Tian et al., 2016).

5. In Line 190, considering the light absorption of methanol soluble organic carbon (MSOC), the optimization of the US IMPROVE algorithm is quite interesting. How did the authors estimate the MSOC concentrations in fine and large size modes?

Response and revisions:

The estimations of fine MSOC and large MSOC concentrations were the same as the calculations of ammonium nitrate (NH_4NO_3), ammonium sulfate ($(NH_4)_2SO_4$) and organic carbon (OM), following the previous studies (Pitchford et al., 2007; Cheng et al., 2015). The concentration of large MSOC was estimated by dividing the total concentration of the component by 20 μg/m^3 (e.g., if the total MSOC concentration was 4 μg/m^3, the large mode concentration was calculated to be one-fifth of 4 μg/m^3 or 0.8 μg/m^3, leaving 3.2 μg/m^3 in the small mode). If the total MSOC concentration exceeds 20 μg/m^3, all of it was assumed to be in the large mode.

6. In Line 190, why did the authors only include those eight variables in this equation? How about other species like coarse particles, sea salt, and soil dust?

Response and revisions:

We thank the reviewer's comment. In this study, the optimization of the US IMPROVE formula was for $PM_{2.5}$, thus the optimization process did not include coarse particles. As indicated in Figure R2 (the response to Question 3 of reviewer 1), the scattering coefficients by sea salt and soil dust accounted for less than 10% of the total $PM_{2.5}$ scattering, suggesting that the two species should have limited contribution to the total scattering coefficient. In order to be concise in the IMPROVE formula optimization and to ensure the stability of the multiple linear regression, therefore, only ammonium sulfate, ammonium nitrate and organic matter were used as independent variables in the regression. We have added the explanation **in lines 459-465 in the revised manuscript**.

7. In Line 214, the authors need to explain the special reason why they applied PMF model in their analysis.

Response and revisions:

We thank the reviewer's comment. The source apportionment technologies include emissions inventory, chemistry transport model and the receptor model, and the receptor model based on aerosol chemistry analysis has been widely used because it is not limited by the uncertainty of emission inventory or meteorology simulation. Principally the receptor models contain two categories, i.e., the models in which source profiles are needed, such as the chemical mass balance (CMB) method, and those in which source profiles are not needed, such as the positive matrix factorization (PMF) method (Yin et al., 2015). Due to lack of sufficient local measurements, it is generally difficult to build comprehensive and accurate source profiles of various aerosol components for individual cities in China. In this work, therefore, we applied the PMF model to exclude the uncertainty of source profiles which were commonly developed based on literatures or measurements across the country. We have added the explanation **in lines 247-252 in the revised manuscript**.

8. In Line 292, the author stated that "the sum of NO_3^-, SO_4^{2-} and OC for the heavily polluted period was 10.7 and 2.9 times greater than those for the lightly polluted and clean periods". Something seems wrong here. In which period was the concentration higher, lightly polluted or clean period? From Table 1, moreover, it seems that SNA was elevated more than OC in the heavily polluted period compared to the clean days. Any reason for this difference?

Response and revisions:

We thank the reviewer's comment. We are sorry for the mistakes and corrected the text as "the sum of NO_3^-, SO_4^{2-} and OC for the heavily polluted period was 2.9 and 10.7 times greater than those for the lightly polluted and clean periods" **in line 328 in the revised manuscript**.

It is correct that SNA concentration was elevated more than OC in the heavily polluted period compared to the clean days in this work. During heavily polluted episodes,

enhancement of sulfate and nitrate levels could be more significant than organic matter because the high relative humidity and precursor emissions (i.e., SO_2 and NO_x) promoted the generation of SNA (Tian et al., 2014). During clean periods (commonly in summer), ammonium nitrate (NH_4NO_3) would dissociate to NH_3 and HNO_3 at high temperatures, while secondary organic carbon (SOC) concentration may be increased due to the high levels of O_3 and solar radiation. Those factors caused the result that SNA was elevated more than OC in the heavily polluted period compared to the clean days. Similar result was found in Beijing, where the mass fraction of SNA in fine particles increased from 19% on non-haze days to 31% on haze days, while that of OM decreased from 38% on non-haze days to 31% on haze days (Tian et al., 2016). We have added the above explanation **in lines 334-342 in the revised manuscript**.

9. The authors did not clearly explain the data of which site were used in Section 3.4. If it is based on the data of the three sites, the assumption in Section 3.4 that chemical particles were externally mixed will cause large uncertainty in the calculation of scattering coefficient at NUIST because the internal mixture was an important particle mixing state at NUIST (Figure 3c).

Response and revisions:

We thank the reviewer's comment. Assuming different aerosol species were externally mixed, the influences of size distribution and pollution levels on aerosol light scattering was analyzed based on the aerosol composition information at the three sites. Although internal mixing was identified as an important particle mixing state at NUIST, the Mie theory cannot simulate the scattering coefficients of individual aerosol chemical components based on the assumption of internal or core-shell mixing but external mixing (Cheng et al., 2015; Ding et al 2015). According to Figure 3c in the revised manuscript, the scattering coefficient estimated with the external mixing assumption was 1.07±0.05 and 1.08±0.06 times of those from the internal mixing state simulation and instrument measurement, respectively. Therefore, the overestimation was smaller than 10% by the aggregated scattering coefficient from those of individual chemical species with an assumption of external mixing at NUIST.

We have added the explanation **in lines 540-545 in the revised manuscript.**

10. In Line 534, in general, results generated from PMF model could be questionable if less than 100 samples were used in the model. How did the authors consider this problem?

Response and revisions:

In this study, the PMF analysis was performed respectively at the three sites for the accumulation mode particles with the size bins from 0.18 to 1.8 μm. The samples used in PMF model were 300, 100 and 124 at NJU, PAES and NUIST, respectively. We thus believe that the sample size was sufficient for the PMF analysis.

References

Cheng, S. H., Yang, L. X., Zhou, X. H., Xue, L. K., Gao, X. M., Zhou, Y., and Wang, W. X.: Size-fractionated water-soluble ions, situ pH and water content in aerosol on hazy days and the influences on visibility impairment in Jinan, China, Atmos. Environ., 45, 4631–4640, doi:10.1016/j.atmosenv.2011.05.057, 2011.

Cheng, Z., Jiang, J., Chen, C., Gao, J., Wang, S., Watson, J.G., Wang, H., Deng, J., Wang, B., Zhou, M.: Estimation of aerosol mass scattering efficiencies under high mass loading: case study for the megacity of Shanghai, China, Environ. Sci. Technol., 49, 831-838, doi:10.1021/es504567q, 2015.

Cui, X., Wang, X., Yang, L., Chen, B., Chen, J., Andersson, A., Gustafsson, Ö.: Radiative absorption enhancement from coatings on black carbon aerosols, Sci. Total Environ., 551-552, 51-56, doi:10.1016/j.scitotenv.2016.02.026, 2016.

Ding, J., Han, S., Zhang, Y., Feng, Y., Wu, J., Shi, G., Wang, J.: Chemical characteristics of particles and light extinction effects in winter in Tianjin, Res. Environ. Sci., 28, 1353-1361, doi:10.13198/j.issn.1001-6929.2015.09.03, 2015.

Massabò, D., Caponi, L., Bove, M.C., Prati, P.: Brown carbon and thermal-optical analysis: A correction based on optical multi-wavelength apportionment of atmospheric aerosols, Atmos. Environ., 125, 119-125, doi:10.1016/j.atmosenv.2015.11.011, 2016.

Pitchford, M., Malm, W., Schichtel, B., Kumar, N., Lowenthal, D., Hand, J.: Revised algorithm for estimating light extinction from IMPROVE particle speciation data, J. Air Waste Manag. Assoc., 57, 1326-1336, doi:10.3155/1047-3289.57.11.1326, 2007.

Tian, S. L., Pan, Y. P., Liu, Z., Wen, T., and Wang, Y. S.: Size-resolved aerosol chemical analysis of extreme haze pollution events during early 2013 in urban Beijing, China, J. Hazard. Mater., 279, 452–460, doi:10.1016/j.jhazmat.2014.07.023, 2014.

Tian, S. L., Pan, Y. P., Wang, Y. S.: Size-resolved source apportionment of particulate matter in urban Beijing during haze and non-haze episodes, Atmos. Chem. Phys., 16, 1-19, doi:10.5194/acp-16-1-2016, 2016.

Yin, J., Cumberland, S. A., Harrison, R. M., Allan, J., Young, D. E., Williams, P. I., and Coe, H.: Receptor modelling of fine particles in southern England using CMB including comparison with AMS-PMF factors, Atmos Chem Phys, 15, 2139-2158, 2015.

Characterization and source apportionment of aerosol light scattering in a typical polluted city in Yangtze River Delta, China

Dong Chen[1, 2], Yu Zhao[1, 3*], Jie Zhang[2, 3], Huan Yu[4], Xingna Yu[4]

1. State Key Laboratory of Pollution Control & Resource Reuse and School of the Environment, Nanjing University, 163 Xianlin Ave., Nanjing, Jiangsu 210023, China

2. Jiangsu Provincial Academy of Environmental Science, 176 North Jiangdong Rd., Nanjing, Jiangsu 210036, China

3. Collaborative Innovation Center of Atmospheric Environment and Equipment Technology, CICAEET, Nanjing, Jiangsu 210044, China

4. School of Environmental Science and Engineering, Nanjing University of Information Science and Technology, Nanjing, Jiangsu 210044, China

*Corresponding author: Yu Zhao

Phone: 86-25-89680650; email: yuzhao@nju.edu.cn

ABSTRACT

Through online observation and offline chemistry analysis of samples at suburban, urban and industrial sites (NJU, PAES and NUIST respectively) in Nanjing, a typical polluted city in Yangtze River Delta, we optimized the aerosol light scattering estimation method, identified its influencing factors, and quantified the contributions of emission sources to aerosol scattering. The daily average concentration of $PM_{2.5}$ during the sampling period (November 2015-March 2017) was 163.1 ± 13.6 μg/m^3 for the heavily polluted period, 3.8 and 1.6 times those for the clean (47.9 ± 15.8 μg/m^3) and lightly polluted (102.1 ± 16.4 μg/m^3) periods, respectively. The largest increase in PM concentration and its major chemical components was found at the size range of 0.56-1.0 μm for the heavily polluted period, and the contributions of nitrate and sulfate were the greatest in the 0.56-1.0 μm fraction (19.4-39.7% and 18.1-34.7% respectively) for all the three periods. The results indicated that the large growth of nitrate and sulfate were one of the major reasons for the polluted periods. Based on measurements at the three sites, the US Interagency Monitoring of Protected Visual Environments (IMPROVE) algorithm was optimized to evaluate aerosol scattering in eastern China. The light-absorption capacity organic carbon (OC) was estimated to account for over half of the methanol soluble organic carbon (MSOC) at NJU and PAES, whereas the fraction was lower at NUIST. Based on Mie theory, we found that the high relative humidity (RH) could largely enhance the light scattering effect of accumulation particles, but it had few effects on the mixing state of particles. The scattering coefficients of particles within the 0.56-1.0 μm range contributed the most to the total scattering (28-69%). The mass scattering efficiency (MSE) of sulfate and nitrate increased with the elevated pollution level, whereas a low MSE of organic matter (OM) was found for the heavily polluted period, probably because a proportion of OM had only light-absorption property. A coupled model of positive matrix factorization (PMF) and Mie theory was developed and applied for the source apportionment of aerosol light scattering. Coal burning, industry and vehicles were identified as the major sources of the reduced visibility in Nanjing, with an estimated

删除的内容: IMPROVE

删除的内容: OC

collective contribution at 64-70%. The comparison between the clean and polluted period suggested that the increased primary particle emissions from vehicles and industry were the major causes of the visibility degradation in urban and industrial regions, respectively. In addition, secondary aerosols were a great contributor to the reduced visibility.

1 INTRODUCTION

Atmospheric aerosols play a great role in visibility degradation, radiative balance variation and climate (Liu et al., 2017; Malm and Hand, 2007; Zhang et al., 2017), resulting largely from their light extinction (Seinfeld and Pandis, 2006). Understanding the contributions of individual chemical species to aerosol light extinction is important for policy making to alleviate the reduced visibility in cities with aerosol pollution. Studies have estimated that the aerosol single scattering albedo (the fraction of light scattering coefficient to the total extinction) ranges from 0.81-0.93 in urban China (Andreae et al., 2008; Cao et al., 2012; Xu et al., 2002; Xu et al., 2012), implying that the deteriorated visibility primarily results from the scattering effect of aerosols.

Aerosol light scattering is greatly affected by its chemical composition and hygroscopic growth (Liu et al., 2008; Tao et al., 2014a). Based on estimation of the mass scattering efficiency (MSE) of different chemical components, previous studies found that nitrate, sulfate, sea salt and organic matter (OM) are the dominant contributors to aerosol scattering. Developed based on the long-term observations in national parks, the US “IMPROVE” (Interagency Monitoring of Protected Visual Environments) algorithm has been applied to calculate the light extinction of chemical species in aerosols (Watson et al., 2002). Two versions of IMPROVE algorithms (IMPROVE1999 and IMPROVE2007 hereinafter) were deduced successively (Lowenthal and Naresh, 2003; Pitchford et al., 2007), and both assumed that OM has no light-absorption capacity and only light-scattering capacity. As part of OM, however, brown carbon (BrC) has been highlighted in recent studies for its light absorption in the near UV region (Alexander et al., 2008; Bond et al., 2006;

Ramanathan et al., 2007; Zhang et al., 2017), and consideration of the light-absorption effect of OM in the optimization process of the IMPROVE formula could improve the understanding of aerosol optical capacity by chemical species (Yan et al., 2014). In addition, hygroscopic growth is a key factor influencing aerosol light scattering (Schwartz, 1996). Previous studies have shown that the light scattering of sulfate and nitrate in $PM_{2.5}$ could be largely enhanced at high relative humidity (RH) conditions (Titos et al., 2016). Aerosol hygroscopicity is expected to depend largely on the particle size and the abundance of water-soluble chemical components (Swietlicki et al., 2008; Tang, 1996). Through the theoretical calculation, Liu et al. (2014) found that smaller particles were in highly hygroscopic mode, whereas larger particles were in nearly hydrophobic mode.

Recently, many studies have been conducted on the relationships between visibility and aerosol light scattering in China (Cheng et al., 2015; Tao et al., 2014b; 2014c; Xue et al., 2010; Zhang et al., 2015). They found the abundance of hygroscopic ammonium nitrate (NH_4NO_3) and ammonium sulfate ($(NH_4)_2SO_4$) in $PM_{2.5}$ and their characteristics were the important reason visibility reduction. However, few studies have analyzed the size distribution of aerosol light scattering or quantified the contributions of different emission source categories to the aerosol light scattering, particularly at the varied air pollution levels. The roles of particles of different sizes and origins on visibility degradation remained unclear. To fill this knowledge gap, this study conducted campaigns at three multiple-functional sites in Nanjing, a mega city located in eastern China. Nanjing suffered relatively heavy aerosol pollution in the Yangtze River Delta (YRD) attrited to the massive emissions of anthropogenic air pollutants (Zhao et al., 2015). The mixed sources of primary aerosols (e.g., coal burning) and secondary aerosol precursors (e.g., vehicle and petrochemical industry) make Nanjing a typical city to study the multiple influential factors of aerosol light scattering (Chen et al., 2019). Combining online and offline techniques at different functional regions, the IMPROVE algorithm was optimized taking the light-absorption OM into account. The influences of aerosol size distributions and pollution levels on the aerosol scattering effect were quantitatively

带格式的：下标
带格式的：下标
带格式的：下标
带格式的：下标
带格式的：下标
删除的内容：NH_4NO_3 and $(NH_4)_2SO_4$

evaluated based on comprehensive analysis of the chemical compositions of particles by size and location. To explore the reasons for the visibility reduction in different functional regions, a new coupled PMF-Mie model was developed and the source apportionments of aerosol light scattering were determined for the clean and polluted periods.

2 METHODOLOGY

2.1 Site description

The campaigns were conducted at three sites in Nanjing, i.e., NJU, PAES and NUIST, representative for the suburban, urban and industrial region, respectively (see the site locations in Figure S1 in the Supplement). NJU (32.07°N, 118.57°E) was on the roof (25 m above the ground) of the School of the Environment building in the Nanjing University campus in eastern suburban Nanjing (Chen et al., 2017; 2019). PAES (32.03°N, 118.44°E) was on the roof (30 m above the ground) of the Jiangsu Provincial Academy of Environmental Science building in western urban Nanjing. The site was surrounded by heavy traffic and commercial and residential buildings (Li et al., 2015). NUIST (32.21°N, 118.72°E) was on the roof of the School of the Environment building in the Nanjing University of Information Science & Technology campus. It was an industrial pollution site influenced by the nearby power, iron & steel, and petrochemical industry plants (Wang et al., 2016a).

2.2 Aerosol sampling and chemical analysis

Pre-combusted (at 500 °C for ~5 h) quartz filters (90 mm in diameter, Whatman International Ltd., UK) were applied for $PM_{2.5}$ sampling. The filter samples were weighed before and after sampling under the constant temperature (23±2°C) and RH (40±3%) for 24 hours conditioning. All the $PM_{2.5}$ samples were collected using the TH-150C sampler (Wuhan Tianhong Ltd., China) at a flow rate of 100 L/min. From November 2015 to March 2017, 282 daily $PM_{2.5}$ samples at the three sites (174 for NJU, 45 for PAES and 63 for NUIST) were collected.

Three sets of ten-stage Micro-Orifice Uniform Deposit Impactors (MOUDI,

Model 110, MSP Corp., USA) were adopted to collect size-segregated particles. The 50% cutoff points of the MOUDI-110 were 18, 10, 5.6, 3.2, 1.8, 1.0, 0.56, 0.32, 0.18 and 0.056 μm. Loaded with Teflon and quartz filters (47 mm in diameter, Whatman International Ltd., UK), MOUDI was operated at a flow rate of 30 L/min. To obtain sufficient particles at each stage for the chemical analysis, every sampling lasted continuously for 24 h from 9:00am. All the MOUDI samplers were cleaned using an ultrasonic bath for 30 min before each sampling. The flow rate was calibrated before each sampling and was monitored with the flow meter during the whole sampling process. Those quality control measures assured that the MOUDI samplers were not blocked during the sampling period and the particles collected in the filter were evenly distributed, even for the heavily polluted period with the $PM_{1.8}$ concentration measured over 120 $\mu g/m^3$ (see the samples in Figure S2 in the supplement). Attributed to weather condition and aerosol sampler maintenance, the sampling periods for the three sites were different. Seventy-five sets of particle samples were obtained from December 2015 to February 2017 at NJU, 25 sets were obtained from August 2016 to January 2017 at PAES, and 31 sets were obtained from July 2016 to February 2017 at NUIST. Simultaneous samplings were conducted at the three sites from one week to ten days in each season from summer 2016 to winter 2016-2017. For the remaining time, two MOUDI samplers were applied to collect Teflon and quartz filter samples simultaneously at one of the three sites. Besides, blank filters were applied to correct the possible bias in the analysis of aerosol chemical species. Totally 19 sets of size-segregated blank filters (10, 4 and 5 for NJU, PAES and NUIST, respectively) and 35 daily blank $PM_{2.5}$ filters (25, 6 and 9 for NJU, PAES and NUIST, respectively) were obtained at the three sites. All the blank filters were put in the samplers without inlet air flow for 24 h when the field campaigns finished. We took NJU as an example to check the consistency between the two types of samplers. As shown in Figure S3 in the supplement, excellent agreement was found between the mass concentrations of $PM_{1.8}$ collected with quartz fiber in MOUDI impactor and $PM_{2.5}$ collected with TH-150 sampler.

Three anions (SO_4^{2-}, NO_3^- and Cl^-) and five cations (Na^+, NH_4^+, K^+, Mg^{2+}, and

删除的内容: , and all

删除的内容: t

删除的内容: sampling

删除的内容: s were

删除的内容: .

带格式的: 下标

带格式的: 上标

带格式的: 下标

删除的内容: Considering the weather, aerosol samples maintenance and other factors, the sample periods for the three sites will be different. Simultaneous sampling were conducted for the three sites in each season to make spatial comparison. For the remaining time of each season, two MOUDI samplers were used to collect Teflon and quartz filter samples simultaneously for source analysis of PM at one of the three sites.

Ca^{2+}) in particles were measured in the extracted solution of the filter samples with ion chromatography (Dx-120, Dionex Ltd., USA). CS12A column (Dionex Ltd.) with 20 mM MSA eluent and AS11-HC column (Dionex Corp.) with 8 mM KOH eluent were used to measured cations and anions, respectively (Chen et al., 2019). Elemental carbon (EC) and organic carbon (OC) were measured with an OC-EC aerosol analyzer (Sunset Inc., USA) following the thermal-optical transmittance (TOT) protocol. In addition to thermal EC and OC, the instrument also provides the optical EC and OC by measuring the light attenuation (ATN). As the ATN is determined not only by EC but also by BrC, the optical method may overestimate EC and underestimate OC (Cui et al., 2016; Massabò et al., 2016). The optical EC and OC were thus not adopted in this work. More details on the analyzer operation were described in our previous studies (Chen et al., 2017; 2019). We used the methanol soluble organic carbon (MSOC) as BrC surrogate. It was believed to be more suitable than water soluble organic carbon (WSOC), as a large fraction of BrC absorption comes from OC insoluble in water (Cheng et al., 2016; 2017; Huang et al., 2018; Lei et al., 2018). The analytical procedure was described in details in Chen et al. (2019). As shown in Figure S4 in the supplement, MSOC was measured to account for 88% of the total OC mass for all the samples in this work, similar to the fraction of 85% by Cheng et al. (2016). Elements of size-resolved particles collected in the Teflon filters (As, Al, Ba, Cd, Co, Cr, Cu, Fe, Mn, Mo, Ni, Ti, V, and Zn) were measured with an inductively coupled plasma-mass spectrometer (ICP-MS, PerkinElmer ELAN 9000, USA) in order to provide further information on the aerosol sources. More detailed information on the instrument was provided by Khan et al. (2016) including the precision, calibration, detection limit, and analytical procedures.

2.3 Measurements of real time aerosol scattering coefficients

The aerosol scattering coefficients were measured using two different types of integrating nephelometers. Two Model Aurora 1000G nephelometers (Ecotech Pty Ltd, Australia) were operated at NJU and PAES at the wavelength of 520 nm, and one Model 3563 nephelometer (TSI Inc., USA) was operated at NUIST at the wavelength

删除的内容:
删除的内容: estimates
删除的内容: an
删除的内容: e
删除的内容: However,
删除的内容: brown carbon (
删除的内容:)
删除的内容: and the measured
删除的内容: then may overestimate to the true value. So, the measured thermal EC and OC were took into our study.
删除的内容: Recent studies indicated that m
删除的内容:
删除的内容: was a
删除的内容: BrC surrogate
删除的内容: and
删除的内容: was thus used in present study
删除的内容:
删除的内容: ,
删除的内容: The t
删除的内容:
删除的内容: , Model Aurora1000G
删除的内容: at NJU and PAES
删除的内容: . The integrating nephelometer
删除的内容: (
删除的内容: ,
删除的内容: had been
删除的内容: used t
删除的内容: o measure the light scattering at three visible wavelengths (450, 550 and 700 nm, and the

of 550 nm. To obtain the dry aerosol scattering coefficient, the three nephelometers controlled the RH of the inflow air under 50% by the heated inlet to mitigate the impact of water vapor on the scattering coefficient. The nephelometers at NJU and PAES were operated at a flow rate of 5 L/min, and that at NUIST was at 20 L/min. Routine maintenance including zero calibration and span check was conducted following the instrument manual.

To explore the RH impact on aerosol light scattering, an online monitoring instrument Cavity Attenuated Phase Shift Albedo monitor (CAPS, Shoreline Science Research Inc., Japan) was used to measure the ambient scattering coefficient at NJU in real ambient conditions. The instrument operates at the wavelength of 530 nm (Onasch et al., 2015; Petzold et al., 2013), and more details on its operation during the campaigns were provided by Chen et al. (2019).

2.4 Data analysis

2.4.1 Estimation of the scattering coefficient of aerosol chemical species with different methods

The details of IMPROVE1999 and IMPROVE2007 are summarized in the Supplement Section A1. Neglecting the light-absorbing effect of BrC, the two algorithms could overestimate the scattering coefficient of OM (Yan et al., 2014). The major difference between the two versions is that the IMPROVE2007 algorithm considers the variety of mass scattering efficiencies due to particle size for $(NH_4)_2SO_4$, NH_4NO_3 and OM. With consideration of the BrC presence, we conducted the multiple linear regression between the measured light scattering components and aerosol scattering coefficient with SPSS 16.0 (Cheng et al., 2011; Tian et al., 2016) to obtain the mass scattering efficiency (MSE). The contributions of sea salt and soil dust were excluded by subtracting their light scattering coefficients from the measured $PM_{2.5}$ one. The $PM_{2.5}$ scattering coefficient can then be estimated statistically based on the concentrations of individual chemical species as Eq. (1):

删除的内容: were adopted in this work.

删除的内容: i.e., Aurora 1000G (Ecotech Pty Ltd., Australia) at NJU and PAES, and Model 3563 (TSI Inc., USA) at NUIST.

删除的内容: In this study

删除的内容: ,

删除的内容: s

删除的内容: s

删除的内容: were conducted to

删除的内容: considering the presence of BrC. SPSS 16.0 was used in this study for multiple linear regression analysis (Cheng et al., 2011). The measured scattering coefficients were subtracted from the scattering coefficients of sea salt, soil dust and coarse particles.

删除的内容: T

删除的内容: scattering coefficient

删除的内容:

带格式的: 下标

$$b_{sca} = a \times f_S(RH)[Small\ (NH_4)_2SO_4] + b \times f_L(RH)[Large\ (NH_4)_2SO_4] + c \times f_S(RH)[Small\ NH_4NO_3] + d \times f_L(RH)[Large\ NH_4NO_3] + e \times ([Small\ OM] - m \times [Small\ MSOC]) + f \times ([Large\ OM] - n \times [Large\ MSOC]) \quad (1)$$

where b_{sca} is the measured $PM_{2.5}$ scattering coefficient excluding the contribution of sea salt and soil dust; a, c and e are the MSEs of $(NH_4)_2SO_4$, NH_4NO_3 and OM (except for light-absorbing BrC) in the small size mode, respectively; b, d and f are the MSEs of $(NH_4)_2SO_4$, NH_4NO_3 and OM (except for light-absorbing BrC) in the large size mode, respectively (definitions of small and large size modes for various aerosol components can be referred to Pitchford et al. (2007)); m and n indicate the mass fractions of light-absorbing BrC to total MSOC in small and large modes, respectively (definitions of small and large size modes of MSOC are the same as other species); $f(RH)$ (including $f_L(RH)$ and $f_S(RH)$) of sulfate and nitrate indicate the scattering hygroscopic growth factor under a given relative humidity (RH), obtained from Pitchford et al. (2007).

In addition to $PM_{2.5}$, the scattering coefficient for particles at a given size ($b_{sca}(RH)$) is calculated with the Mie theory (Bohren et al., 1998; Cheng et al., 2015):

$$b_{sca}(RH) = \int \pi [D_p \times \frac{g(RH)}{2}]^2 \times Q_{sca}[m(RH),\ Dp,\ \lambda] \times N(D_p) \times g(RH) dD_p \quad (2)$$

where $m(RH)$ is the aerosol refractive index; $g(RH)$ is the hygroscopic growth factor; Q_{sca} is the scattering efficiency for a single spherical particle with diameter D_p and can be calculated with the Mie theory by inputting D_p, $m(RH)$ and the incident wavelength (λ); $N(D_p)$ is the number concentration of particle with diameter D_p. In general, three typical models are proposed to represent the particle mixing state including internal, external and core-shell mixture (Jacobson, 2001; Seinfeld and Pandis, 2006). The methods of calculating the parameters including $m(RH)$ and $N(D_p)$ are different for the three mixed states, and the details can be referred to Ding et al. (2015).

2.4.2 Source apportionment of aerosol scattering coefficients with a coupled model of PMF and Mie theory

Positive matrix factorization (PMF) is an effective technology for source

删除的内容: Malm et al

删除的内容: .

删除的内容: P

删除的内容: ical method

apportionment of atmospheric aerosols (Kim and Hopke, 2004). PMF does not require the source profile (i.e., the aerosol chemistry speciation by source category) as a model input, and thus excludes the uncertainty of source profiles which were commonly developed based on literatures or measurements across the country in China. In this study, PMF 5.0 software was applied for the source apportionment of accumulated mode particles. In total, 245, 145 and 163 aerosol samples were analyzed at NJU, PAES and NUIST, respectively. It is currently difficult to resolve the sources of secondary organic aerosol (SOA) with PMF. In this study, a simplified method was applied to differentiate the sources of primary and secondary aerosols. Organic carbon is split into primary and secondary organic carbon (POC and SOC), and the SOC concentration was calculated with the EC-tracer method (Chen et al., 2017). The source contributions of primary particles were obtained using the PMF model, and those of secondary inorganic aerosol (SIA) and SOA were further determined based on estimates of the nitrogen oxides (NO_x), sulfur dioxide (SO_2) and volatile organic compounds (VOCs) emissions in a local inventory (Huang, 2018; Lang et al., 2017; Wang et al., 2015). The chemical components applied in the PMF model included inorganic ions, carbonaceous components and metallic elements. We followed the method described in the PMF manual and Tian et al. (2016) to calculate the chemical component uncertainties in the measurement dataset. Criteria including the optimum number of factors and the minimization of an objective function Q were determined based on the principles described in previous studies (Moon et al., 2008; Tian et al., 2016; Watson et al., 2015) and applied in the model to obtain the best PMF solution.

A coupled model combining PMF and the Mie theory was developed to evaluate the sources of aerosol light scattering. The procedure of the method was as follows: (1) the EPA-PMF model was applied to quantify the contributions of different sources to the mass concentrations of chemical species in size-segregated particles; (2) the contribution (%) of the i^{th} chemical component to the aerosol scattering coefficient at size D_p was estimated based on Mie theory; (3) the percentage contribution (%) of the i^{th} component in the j^{th} source category to the total scattering at size D_p was calculated as the product of the percentage contribution (%) of the i^{th} chemical species to the

删除的内容: in

total scattering and that of the j^{th} source category to the mass concentration of the i^{th} species in the particles at size D_p, as indicated in Eq.(3); and (4) the percentage contribution (%) of the j^{th} source to the total scattering at size D_p was estimated by summing η_{ijDp}, as shown in Eq. (4).

$$\eta_{ijDp} = a_{ijDp} \cdot \frac{b_{iDp}}{\sum_{i=1}^{m} b_{iDp}} \times 100\% \quad (3)$$

$$\eta_{jD_p} = \sum_{i=1}^{I} \eta_{ijD_p} \quad (4)$$

where i and j stand for the numbers of aerosol chemical components and potential sources, respectively; η_{ijDp} (%) is the contribution (%) of i^{th} scattering component in the j^{th} source to the total particle scattering at size D_p; η_j (%) is the contribution (%) of the j^{th} source to the total scattering at size D_p; a_{ijDp} is the relative contribution (%) of the j^{th} source to the i^{th} chemical component in particles with size D_p from PMF modeling; and b_{iDp} is the contribution of the i^{th} chemical component to the total scattering from Mie modeling.

3 RESULTS AND DISCUSSION

3.1 Mass concentrations and size distributions of PM compositions

Based on the national definition on ambient Air Quality Index (AQI) (MEP, 2012), we divided the whole sampling period into three categories, i.e., the clean period with AQI less than 100, the lightly polluted period with AQI between 100 and 200, and the heavily polluted period with AQI above 200. Note that the AQI is a unitless index calculated based on the daily concentrations of regulated air pollutants including NO_2, SO_2, CO, O_3, $PM_{2.5}$ and PM_{10} (MEP, 2012). As summarized in Table 1, the average daily $PM_{2.5}$ mass concentrations at the three conditions were calculated at 47.9 ± 15.8, 102.1 ± 16.4, and 163.1 ± 13.6 μg/m^3, respectively. The mass concentration of secondary inorganic ions (SO_4^{2-}, NO_3^- and NH_4^+) for the heavily polluted period was 4.4 and 2.2 times those for the clean and lightly polluted periods, respectively. The corresponding values for the carbonaceous aerosols (the sum of OC

and EC) were 3.1 and 1.9 times, respectively, and the OC to EC ratios increased from 4.5 for the clean period to 5.2 for the heavy period. In addition to the particulate components, gaseous pollutants such as NO_2 and SO_2 were also significantly elevated from the clean to the heavy periods. These results imply that secondary aerosol formation was an important source of enhanced $PM_{2.5}$ for the heavily polluted period.

Figure S5 in the Supplement compares the size distributions of mass concentrations for particles and selected chemical components under three pollution levels. Bimodal size distributions were found for PM and OC mass concentrations, with the two peaks at the ranges of 0.56-1.0 μm and 3.2-5.6 μm, respectively. This bimodal pattern could partly result from the coexistence of primary and secondary sources of OC. POC with larger sizes may contribute largely to the peak in the coarser particles. In contrast, due to chemistry reactions of biogenic and anthropogenic VOCs, SOC was expected to be abundant in the accumulation mode (0.18-1.8 μm) (Cao et al., 2007). The size distributions of NO_3^- and SO_4^{2-} followed a unimodal distribution with the mass concentrations peak at the range of 0.56-1.0 μm, as most of the inorganic aerosols were generated through secondary formation. The mass concentrations of PM, NO_3^-, SO_4^{2-} and OC for all sizes were enhanced from the clean to the polluted periods, and the biggest differences were found in the size bin of 0.56-1.0 μm. As shown in Figure S5a, the concentrations of $PM_{0.56-1.0}$ for the heavily and lightly pollution periods were 7.0 and 2.7 times greater than that for the clean period, respectively. Moreover, $PM_{0.56-1.0}$ contributed 31%, 23%, and 15% to the total mass concentrations of particles for the heavily, lightly polluted and clean periods, respectively, implying that the enhanced concentration of $PM_{0.56-1.0}$ was an important reason for the aggravated pollution. As shown in Figure S5b-S5d, the sum of NO_3^-, SO_4^{2-} and OC for the heavily polluted period was 2.9 and 10.7 times greater than those for the lightly polluted and clean periods, respectively. From clean to heavily polluted periods, the collective mass fraction of the three components to $PM_{0.56-1.0}$ increased from 42% to 64%. The results indicated that the increased NO_3^-, SO_4^{2-} and OC at the size bin of 0.56-1.0 μm could be an indicator for the serious air pollution events. As indicated in Table 1, moreover, SNA was elevated more than OC in the heavily

删除的内容: S2

删除的内容: S2a

删除的内容: S2b

删除的内容: S2d

删除的内容: 10.7 and 2.9

删除的内容: According to Table 1,

polluted period compared to the clean days. During the heavily polluted episodes in winter, enhancement of SO_4^{2-} and NO_3^- could be more significant than OM because the high relative humidity and precursor emissions promoted the generation of SNA (Tian et al., 2014). During clean periods (commonly in summer), NH_4NO_3 would dissociate to NH_3 and HNO_3 at high temperature, while the SOC concentration might increase due to the high levels of O_3 and solar radiation. Similar result was found in Beijing, where the mass fraction of SNA was observed to increase from 19% on non-haze days to 31% on haze days, while that of OM decreased from 38% to 31% (Tian et al., 2016).

To explore the mass fractions of major chemical species in the particles, the PM mass was reconstructed as $(NH_4)_2SO_4$ ($1.38\times SO_4^{2-}$), NH_4NO_3 ($1.29\times NO_3^-$), OM ($1.55\times OC$), fine soil (FS) and EC (Cheng et al., 2015; Pitchford et al., 2007). As shown in Figure S6 in the Supplement, strong correlations were found between the reconstructed PM mass concentrations and the measurements for $PM_{1.8}$ (R^2=0.91) and PM_{10} (R^2=0.89) at the three sites. The slope of $PM_{1.8}$ (0.85) was greater than that of PM_{10} (0.72), indicating smaller unidentified fraction in the $PM_{1.8}$. The larger unidentified mass in the reconstructed PM_{10} was probably due to underestimation in the crustal components (Hueglin et al., 2005).

Figure 1 presents the mass concentrations and fractions of the reconstructed aerosol chemical species by particle size under the three pollution levels. NH_4NO_3, $(NH_4)_2SO_4$, and OM were the dominant components in particles. From the clean to heavily polluted periods, their mass fractions to $PM_{1.8}$ increased from 16.9 to 35.3%, from 14.9 to 28.6% and from 16.7 to 22.2%, respectively (Figure 1b, Figure 1d and Figure 1f). The mass fraction of OM in $PM_{1.8}$ was 5.4% and 7.4% larger than NH_4NO_3 and $(NH_4)_2SO_4$ for the clean period, while 13.3% and 6.6% smaller than those for the heavily polluted period, respectively. The results further confirmed that substantial growth in the mass of NH_4NO_3 and $(NH_4)_2SO_4$ was an important reason for the aerosol pollution. The formation of sulfate, nitrate, and ammonium (SNA) is mainly affected by the emissions of precursors and the atmospheric oxidation capacity Due to the great use of fossil fuel consumption, the emissions of precursors SO_2 and

删除的内容: In this study, the concentrations of PM and its chemical components were higher in winter and lower in summer, due to a combination of emissions and seasonal variance in ...
删除的内容: sulfate
删除的内容: nitrate
删除的内容:
删除的内容: were
删除的内容: organic matter
删除的内容: (i.e., SO_2 and NOx)
带格式的: 下标
删除的内容: ammonium nitrate (
带格式的: 下标
带格式的: 下标
删除的内容:)
带格式的: 下标
带格式的: 下标
删除的内容: s
删除的内容: secondary organic ...
删除的内容: ay
删除的内容: be
删除的内容: d by
带格式的: 下标
删除的内容: concentration
删除的内容: These factors caused the ...
删除的内容: dominated in fine ...
删除的内容: d
删除的内容: .1
删除的内容: .2
删除的内容: 7.9
删除的内容: on
删除的内容: non-haze days
删除的内容: .2
删除的内容: on haze days
删除的内容: S3

500 NO_X per unit area in eastern China were estimated 2.3 and 3.4 times larger than the
501 national average, respectively (Cheng et al., 2012; Shi et al., 2014). Under high RH,
502 moreover, the SNA formation could significantly be elevated through gas-to-particle
503 heterogeneous reactions for the heavily polluted period (Seinfeld and Pandis, 2006).
504 Sulfate mass concentration, for example, increased from 6.4 μg/m^3 for the clean
505 period to 53.3 μg/m^3 for the heavily polluted period. Among all the size bins,
506 NH_4NO_3 and $(NH_4)_2SO_4$ were estimated to contribute the most to the mass
507 concentrations for 0.56-1.0 μm particles, with their mass fraction ranging 19.4-39.7%
508 and 18.1-34.7%, respectively, across different pollution levels. In comparison, the
509 largest contributions of OM appeared in the 0.056-0.18 μm fraction and were 31.2%,
510 29.0% and 52.3% for the clean, lightly polluted and heavily polluted periods,
511 respectively. As the largest PM fraction was found in the 0.56-1.0 μm size bin for the
512 heavily pollution period, the elevated concentrations of NH_4NO_3 and $(NH_4)_2SO_4$ in
513 $PM_{0.56-1.0}$ were the major causes of the increased aerosol pollution.
514 Figure S7 in the Supplement compares the size distributions of PM mass
515 concentrations and selected chemical species at the three sites. As mentioned above, a
516 bimodal distribution with two peaks at 0.56-1.0 μm and 3.2-5.6 μm was observed for
517 PM and OC at all the three sites, attributed to the coexistence of primary and
518 secondary sources. Different from PAES and NUIST, NO_3^- had an obvious small
519 coarse mode peak at NJU. Previous studies suggested that the chemistry of coarse
520 mode NO_3^- can vary in different locations, and the components include NH_4NO_3,
521 $NaNO_3$ and $Ca(NO_3)_2$ (Pakkanen et al., 1996). As NJU was close to the G25 highway,
522 the reaction of HNO_3 with crustal particles could be an important process for coarse
523 mode NO_3^- formation. The highest mean concentrations of NO_3^- and SO_4^{2-} at the
524 0.56-1.0 μm size among the three sites were observed at NJU, followed by NUIST
525 and PAES. As NO_3^- and SO_4^{2-} were the major components of the aerosol light
526 scattering, the variety of their mass concentrations at 0.56-1.0 μm could be a crucial
527 reason for the visibility difference among the three sites. A greater difference was
528 found for the size distribution of OC among the three sites, and the highest
529 concentration at the 0.56-1.8 μm size was observed at NUIST. Our previous work

删除的内容: S4

found that NUIST was greatly influenced by VOCs emissions of surrounding industrial plants (Chen et al., 2019). Given its capability of light scattering and absorption, the abundant OC in the area could play an important role on the visibility.

3.2 Evaluation and optimization of the IMPROVE algorithm

Figure S8 in the Supplement presents the linear regressions between the measured daily aerosol scattering coefficients with nephelometers ($b_{sp\text{-}m}$) and those calculated with IMPROVE algorithms ($b_{sp\text{-}1999}$ and $b_{sp\text{-}2007}$) based on the measured concentrations of particle components at the three sites. At each site, strong correlations were found between the observation and IMPROVE estimation ($R^2 \geq 0.94$), indicating consistency between the different techniques. As shown in Figure S8a, the calculated aerosol scattering coefficients $b_{sp\text{-}1999}$ were 30%, 16% and 19% smaller than the measured values at NJU, PAES and NUIST, respectively. Similar results were found for other megacities in eastern China. Based on the online analytical methods, for example, Cheng et al. (2015) estimated that the scattering coefficients predicted by the IMPROVE1999 algorithm were 34% smaller than the measurement for a heavy pollution period in Shanghai. A greater underestimation of the scattering coefficient existed at NJU than the other two sites, partly due to the relatively abundance of sulfate and nitrate in particles at NJU. The sum of SO_4^{2-} and NO_3^- accounted for 35.3 ± 13.2% of the total mass concentrations of $PM_{2.5}$ at NJU, larger than the fraction at PAES (27.6 ± 12.9%) and NUIST (24.1 ± 11.6%) (note the SO_4^{2-} and NO_3^- concentrations at the 0.56-1.0 μm were the largest at NJU as well, as shown in Figure S7). Tao et al. (2014b) and Cheng et al. (2015) suggested that the relatively small MSE of sulfate and nitrate aerosols in the IMPROVE1999 algorithm might result in underestimation of the scattering coefficient in China, as sulfate and nitrate were the main light-scattering components in $PM_{2.5}$.

As shown in Figure S8b, $b_{sp\text{-}2007}$ was only 4% smaller than the measurement at NJU, and 4% and 18% larger at PAES and NUIST, respectively. Overall, the performance of the IMPROVE2007 algorithm was better than that of the IMPROVE1999, although deviation still existed due to the uncertainty in MSEs for

删除的内容: S5

删除的内容: the three

删除的内容: CAPS

删除的内容: S5a

删除的内容: S4

删除的内容: S5b

chemical species and the presence of light absorption organic matter such as BrC. A relatively large deviation between $b_{sp\text{-}m}$ and $b_{sp\text{-}2007}$ was found at NUIST compared to NJU and PAES. Chen et al. (2019) and Shao et al. (2016) found higher annual average concentration of non-methane hydrocarbon at NUIST (34.4 ppbv) than NJU (22.0 ppbv) or PAES (27.1 ppbv). The more VOCs in the atmosphere were expected to increase the SOC formation and to result in big deviation of $b_{sp\text{-}2007}$, as the OM with light-absorption capability was not considered in IMPROVE2007.

Using the optimized IMPROVE algorithm as described in Section 2.4.1, the aerosol scattering coefficients were recalculated and compared against the observation at the three sites, as illustrated in Figure 2. Good correlations were found between the observed and calculated scattering coefficients at all the sites ($R^2 \geq 0.96$), and the regression slopes were estimated to be much closer to 1 than those between observations and predictions with the IMPROVE1999 or IMPROVE2007 algorithms (Figure S8). In addition, the MSEs calculated based on the Mie theory were applied to evaluate the results of the IMPROVE algorithms. As presented in Figure S9 in the Supplement, the MSEs of $(NH_4)_2SO_4$ and NH_4NO_3 calculated with the optimized IMPROVE algorithm were closer to the MSE simulated by Mie theory than those with the IMPROVE2007 algorithm. The results indicated the optimized algorithm had a better performance and could reduce the bias from the US IMPROVE algorithm.

删除的内容: S5

删除的内容: S6

As summarized in Table 2, the MSEs estimated with the optimized IMPROVE algorithm were 2.29, 4.82, 2.62, 5.35, 4.46, and 6.41 m^2/g for small sulfate, large sulfate, small nitrate, large nitrate, small and large OM, respectively. In comparison, the MSEs for the small and large size modes using the IMPROVE2007 were 2.2 and 4.8 m^2/g for $(NH_4)_2SO_4$, respectively, and 2.4 and 5.1 m^2/g for NH_4NO_3, respectively. The slightly larger MSEs from the optimized IMPROVE algorithm for $(NH_4)_2SO_4$ and NH_4NO_3 implied underestimation of the scattering coefficients of inorganic components when applying the previous algorithm. There were clear differences in the MSEs of OM (especially for fine OM) between the two algorithms, resulting from consideration of the light-absorbed OM in the optimized algorithm. Indicated by the m values in Table 2, the light-absorbed OC accounted for 66% and 71% of the fine

MSOC mass at NJU and PAES, respectively, indicating that most of the fine MSOC had only light-absorption capacity. Unlike NJU and PAES, less than half of the fine MSOC (39%) had light-absorption capacity at NUIST, likely resulting from the varied sources of OM at the three sites. As described in our previous study (Chen et al., 2019), substantial OC was from the secondary formation in industrial polluted region, and its light-absorption capacity was weaker than that from the primary emissions.

In this study, the optimized IMPROVE algorithm for $PM_{2.5}$ did not include the contribution of sea salt or soil dust. As illustrated in Figure S10 in the supplement, sea salt and soil dust accounted collectively for less than 10% of the total $PM_{2.5}$ scattering coefficient, suggesting that the two species should have limited impact on the IMPROVE algorithm optimization. In order to be concise in the optimized formula and to ensure the stability of the multiple linear regression, therefore, only $(NH_4)_2SO_4$, NH_3NO_3 and OM were used as independent variables. Through field measurement and data reconstruction in different cities, previous studies explored the concentrations of $PM_{2.5}$ and its chemical components for various cities in China (Chen et al., 2019; Feng et al., 2012; Lai et al., 2016; Tao et al., 2013., Yang et al., 2011; Zhao et al., 2013). The major components of light scattering in aerosols, SNA, were found to typically account for half of the $PM_{2.5}$ mass concentrations in eastern Chinese cities like Nanjing, Shanghai, and Jinan (Yang et al., 2011). Given the similar SNA levels and strong regional transport of pollution among those cities, the optimized IMPROVE algorithm applied in Nanjing in this work is believed to be more suitable than the previous algorithms for eastern China. Moreover, for other regions with rapidly developing economy and fast industrialization in China including Beijing-Tianjin-Hebei or Pearl River Delta regions, the current work provides methodology and data support for the studies of aerosol light scattering in cities with relatively serious aerosol pollution. Given the fast changes in emission control and aerosol pollution in those regions, more campaigns on aerosol optical and chemical properties are recommended to further evaluate and improve the applicability of the optimized IMPROVE algorithm.

带格式的: 下标
带格式的: 下标
带格式的: 下标
带格式的: 下标
删除的内容: .
删除的内容: was
删除的内容: level
带格式的: 字体: (默认) Times New Roman, (中文) 黑体, 字体颜色: 自动设置
带格式的: 字体: (默认) Times New Roman, (中文) 黑体, 字体颜色: 自动设置
带格式的: 字体: (默认) Times New Roman, (中文) 黑体, 字体颜色: 自动设置
带格式的: 缩进: 首行缩进: 0 字符

3.3 Effects of mixing state and relative humidity on aerosol light scattering

Figure 3 presents the scattering coefficients measured by nephelometer and those simulated by Mie theory at the three sites under dry conditions (RH < 40%). The simulated scattering coefficients based on the assumption of an external mixing state were larger than those based on core-shell and internal mixing states at all the three sites. Compared with the internal and core-shell states, the simulated scattering coefficients in the external mixing state were closer to the measurements at NJU and PAES (Figure 3a and 3b), indicating the reasonable assumption of external mixtures as the main mixing state of particles. Similarly, Ma et al. (2012) also suggested that the external mixture was an important particle mixing state in northern China based on a stochastic particle-resolved aerosol box model. Assuming the aerosol components were externally mixed, Cheng et al. (2015) estimated the MSEs of aerosol species in Shanghai, and found better agreement between the optimized scattering coefficients and the measurements. At NUIST, the measured scattering coefficients were closer to the simulated values in internal and core-shell states, likely due to the high aging level of SOA at the industrial site (Figure 3c). Due to the strong atmospheric oxidation and thereby the abundance of SOA coatings at NUIST, our previous study suggested that the aerosol aging process could result in the growth of internally mixed BC (Chen et al., 2019). Based on the observation of O_3 and percentage of internally mixed BC, Lan et al. (2013) suggested that photochemical production of secondary aerosol components was the main reason for the switching from an external mixing state to an internal mixing state for BC.

In an actual environment, ambient aerosols are typically hygroscopic under the conditions of high RH, and it is an important reason for visibility degradation. Table S1 in the Supplement summarizes the growth factors (GF) of particle size measured in Nanjing at different RH levels in previous studies. To evaluate the rationality of those GF values, we followed the method by Tao et al. (2014b) and calculated the scattering hygroscopic growth factor (f(RH)) at NJU based on the measured ambient scattering coefficients by CAPS and the dry scattering coefficients by nephelometer, as shown in Figure S11 in the Supplement. The correlation between f(RH) and RH was fitted

删除的内容: S7

through the power regression. Figure S12 in the Supplement presents a good agreement between the scattering coefficients estimated by f(RH) and those obtained by the Mie theory (R^2=0.95). The results indicate the accuracy of the GF values applied on different particle sizes and RH levels. The estimated and measured scattering coefficients at NJU under ambient condition are shown in Figure S13 in the Supplement. Different from the estimation under the dry conditions, the lowest value was found for the externally mixing state among the three mixing modes. In the externally mixing state, only sulfate and nitrate particles had hygroscopicity under wet conditions, whereas each particle had the capability of hygroscopic growth in the internal mixing and core-shell states, resulting in a significant increment in the scattering coefficient. Similarly, comparing the measured scattering coefficients under the dry and ambient conditions (Figure 3 and Figure S13), the simulated values based on an external mixing state were closer to the measurements than the other two modes, implying that RH had a limited effect on the particle mixing state.

To explore the impact of RH on the light scattering of particles with different sizes, the size distribution of f(RH) was estimate and shown in Figure 4. Large differences were found between f(RH) when the RH was above and below 75%, and high RH enhanced the capacity of scattering hygroscopicity growth of small size particles. Approximately 140 nm particles had strong hygroscopicity when the RH was below 75%, whereas a high f(RH) (1.41±0.03) was observed for the accumulation mode particles from 100 to 400 nm when the RH was above 75%. Similar results were reported for Beijing: larger hygroscopic GF was measured for accumulation mode particles (100–300 nm) with a hygroscopicity tandem differential mobility analyzer (H-TDMA), consistent with the elevated abundance of the light-scattering compositions such as sulfate and nitrate (Meier et al., 2009).

3.4 Size distribution of aerosol light scattering by pollution level

Figure 5 shows the size distribution of the scattering coefficients for particles and given chemical components under the three pollution levels, based on the measurements at all the three sites. Note the result was obtained with Mie theory

删除的内容: S8

删除的内容: S9

删除的内容: S9

删除的内容: .

under the assumption of external mixing at ambient condition. Although other mixing states might be more important at specific site (e.g., internal mixing at NUIST), their influence on scattering coefficient estimation was modest (Figure 3). The scattering coefficients of particles for all size categories were the largest for the heavily polluted period (Figure 5a). The accumulation mode particles (0.18-1.8 μm) accounted for 92.9%, 92.6 and 93.4% of the total scattering coefficients for the clean, lightly polluted and heavily polluted periods, respectively. In particular, particles in the size bin of 0.56-1.0 μm accounted for 57% and 63% of the scattering coefficient for the heavily and lightly polluted periods, respectively, much larger than that for the clean period, 38%. From the results of Section 3.1, the abundance of particles of different sizes was considered to be an important factor for the variety of scattering coefficients across the whole size range.

As the dominant chemical components of aerosol light scattering, $(NH_4)_2SO_4$, NH_4NO_3 and OM collectively contributed 90%, 76% and 60% to the mass concentrations of $PM_{0.56\text{-}1.0}$ for the heavily polluted, lightly polluted and clean periods, respectively (Figure S5b-S5d). The scattering coefficients of $(NH_4)_2SO_4$ and NH_4NO_3 were the largest in the size bin of 0.56-1.0 μm for the three pollution levels, and their contributions increased along with the aggravation of pollution (Figure 5b and Figure 5c). The OM concentration in the size bin of 0.56-1.0 μm was 2.5 $\mu g/m^3$ for the clean period, and those for the lightly and heavily polluted periods were 160% and 510% larger, respectively. The scattering coefficient of OM in the size bin of 0.56-1.0 μm for the heavily polluted period was 15% less than that for the lightly polluted period, indicating the more important role of OM in the particle scattering effect for the lightly polluted period (Figure 5d). The large OM scattering contribution could likely be explained by the elevated mass fraction of OM and/or enhancement of the OM MSE. It could be inferred that the low visibility during heavy pollution resulted mainly from the enhancement of the scattering effect of SNA.

The MSEs of given chemical components in $PM_{1.8}$ are presented by pollution level in Figure 6. Increased MSEs for $(NH_4)_2SO_4$ and NH_4NO_3 were found along with the elevated $PM_{2.5}$ pollutions (Figure 6a). The large contributions of inorganic

删除的内容: .

删除的内容: at ambient condition

删除的内容: S2b

删除的内容: S2d

components and their strong light scattering ability were important reason for the reduced visibility during the heavily polluted period. Although the largest OM concentrations were observed in each size bin for the heavy pollution period, the smallest MSE of OM in $PM_{1.8}$ was found for the heavily polluted period (3.73 m^2/g, Figure 6b). As discussed in Section 3.2, most of the fine MSOC was expected to have only a light-absorption effect whereas large MSOC had light-scattering capability. With the optimized IMPROVE algorithm, the mass fraction of light-absorption OC to total MSOC mass was estimated at 66.9±5.8% for the heavily polluted period, much larger than those for clean and lightly polluted periods at 44.3±6.5% and 50.8±5.9%, respectively, as shown in Figure S14 in the Supplement. Therefore, the small MSE of OM for the heavily polluted period was partly attributed to the abundance of light absorption BrC in $PM_{2.5}$.

For the whole research period, the MSEs of $(NH_4)_2SO_4$, NH_4NO_3 and OM in $PM_{1.8}$ were calculated at 3.95, 4.26 and 4.14 m^2/g with the Mie theory, while the analogue numbers in $PM_{2.5}$ were 3.94, 4.31 and 5.25 with the optimized IMPROVE algorithm, respectively (Table 2). Very good agreement between the two methods was found for SNA, and clearer discrepancy existed for OM, indicating a larger uncertainty in the evaluation of organic aerosol scattering.

3.5 Source apportionment of aerosol light scattering with the PMF-Mie coupled model

As illustrated in Figure 5, the light scattering of the accumulation mode (0.18-1.8 μm) accounted for the largest proportion of the total light scattering. To better understand the causes of visibility degradation, the source apportionment of aerosol light scattering at this size range was conducted for different pollution levels with the PMF and Mie coupled model, as described in Section 2.4.2. The PMF model was adopted to identify the potential sources and to estimate their respective contributions to the mass concentration of accumulation mode particles. To resolve the appropriate number of factors, different numbers of identifiable sources were tested. The source profiles and contributions to accumulation mode particles at the three sites are

删除的内容: S10

删除的内容: Mien

删除的内容: results of the

删除的内容: their

764 presented in Figure S15 in the Supplement and Figure 7a-c, respectively. The main
765 sources identified at the three sites include coal combustion, industrial pollution,
766 vehicle, fugitive dust, biomass burning, and SIA (Figure S15). Compared to NJU and
767 NUIST, vehicle contributed more to accumulated particles at the urban site PAES
768 (Figure 7b). As stated in Section 2.4, we assumed that the contribution of the
769 individual source category to the secondary particle component was proportional to
770 the fraction of that source category to the emissions of corresponding precursors
771 (Lang et al., 2017). Based on the emission inventory of precursors of SOC (VOCs)
772 and SIA (NO_x, SO_2 and NH_3) in Nanjing (Huang, 2018), the source apportionment for
773 primary and secondary particles of accumulation mode at the three sites were
774 estimated, and the results are presented in Tables S2-S4 in the Supplement. With the
775 source apportionment of secondary components, the contributions of coal combustion
776 and industrial pollution increased 45-50% and 138-478% compared to those for
777 primary particles across the three sites, respectively. The result indicates that the
778 gaseous precursors from coal combustion and industrial pollution greatly elevate the
779 aerosol pollution.

780 The contributions of different aerosol species to the aerosol light scattering were
781 estimated using the Mie model, and the results are presented in Table S5 in the
782 Supplement. OM contributed the most to the total scattering at the three sites (31%,
783 29% and 33% for NJU, PAES and NUIST, respectively). Compared to other Chinese
784 mega cities, the contribution of OM in Nanjing was close to that for inland cities like
785 Beijing (Tao et al., 2015) and Tianjin (Wang et al., 2016b), but was much larger than
786 that observed in a coastal megacity, Guangzhou (Tao et al., 2014c).

787 Combined with the source apportionment from the PMF model, Figure 7d-7f
788 illustrates the source contribution to aerosol light scattering at the three sites. Coal
789 combustion, industrial plants and vehicle were the major sources of the aerosol light
790 scattering in Nanjing, and the three source categories collectively accounted for
791 64-70% of the total scattering capacity of aerosols. Given their relatively intensive
792 activities in urban and industrial regions, vehicles and industrial plants were identified
793 as the largest contribution sources at PAES and NUIST, respectively. Indicated by the

删除的内容: S11

删除的内容: S11

删除的内容: PME

dashed lines in Figure 7d-7f, the collective contributions of secondary aerosol components were estimated to be 26.7%-35.2% of the total scattering at the three sites, suggesting the important role of secondary aerosol formation in visibility reduction.

Figure 8 illustrates the source apportionment of aerosol light scattering for the clean and polluted periods at the three sites. Coal combustion contributed the most to the total scattering for the clean period, and the contribution declined significantly for the polluted period, from 39% to 21%, from 38% to 19% and from 35% to 18% at NJU, PAES and NUIST, respectively. The results implied that coal combustion might not be the most important reason for visibility degradation in polluted periods. Similarly, the contribution of fugitive dust during the polluted period was estimated to be smaller than that for the clean condition. In contrast, the contributions of vehicles and industrial pollution to light scattering increased from 27% to 48%, from 27% to 47% and from 31% to 62% for the polluted periods compared to the clean period at NJU, PAES, and NUIST, respectively. As shown in Figure 8b and 8c, particularly, the contribution of primary emissions from vehicles to aerosol scattering was estimated to increase from 11.4% to 21.5% at PAES, and that from industrial plants increased from 4.5% to 13.5% at NUIST. The primary aerosol emissions from vehicles and industrial plants were thus identified as the main cause of visibility reduction in the urban and industrial areas, respectively. Similarly, Wang et al. (2016b) suggested that vehicle was the dominate source of aerosol light extinction in Hangzhou, with the contribution to the total extinction coefficient of $PM_{2.5}$ reaching 30.2%. The present study indicated that more effective measures for reducing the primary particle emissions from vehicles and industrial production should be conducted to avoid severe haze pollution in urban and industrial regions.

In addition, the results suggest that secondary aerosols were another important contributor to the reduced visibility. From the clean to the heavily polluted periods, as shown in Figure 8, the contributions of secondary aerosols to the total light scattering increased from 19.9% to 36.7%, from 20.9% to 32.4%, and from 28.6% to 41.7% at NJU, PAES, and NUIST, respectively. As shown in Table 3, the contributions of SIA to the total scattering at the three sites were ranged at 14.5%-19.9% and 24.5%-28.0%,

much more than those of SOA at 4.1%-8.7% and 7.9%-13.7% for the clean and polluted periods, respectively. The results imply that SIA had a greater impact on visibility degradation. Although the contribution of coal combustion to the total scattering declined from clean to polluted periods, the contributions of SIA from coal combustion for the polluted periods were 88%, 35% and 36% larger than those for the clean period at NJU, PAES and NUIST, respectively. The enhancement of SIA from coal combustion was thus an important cause of polluted days. Moreover, the contribution of SOA to the total scattering coefficient during the polluted periods was estimated at 13.7% at NUIST, larger than the 7.9% and 9.1% at PAES and NJU, respectively, indicating that the contribution of SOA to visibility reduction at industrial polluted areas should not be ignored. Notably, there is uncertainty in the methodology of source apportionment of aerosol scattering coefficients. In particular, the assumption that the secondary components were proportional to the emissions of their precursors is a simplified method and probably led to large bias, as the complicated nonlinear mechanism of secondary aerosol formation is not recognized. To further reduces the uncertainty and to improve the source apportionment, some specific tracers of secondary aerosols like semi-volatile and low-volatile oxygen-containing organic aerosols can be observed with advanced technology such as aerosol mass spectrometry (AMS), and the observation data can then be combined with the receptor models to quantify the source contribution of secondary aerosols. Besides, air quality model that integrates particle source apportionment technology (PSAT) is recommended to be applied to evaluate and confirm the performance of the source apportionment of secondary aerosols with the receptor model.

删除的内容: More tools including chemistry transport modeling and radiocarbon measurements are thus recommended to be integrated into future studies to better determine the primary and secondary sources of aerosols.

4 CONCLUSIONS

A comprehensive investigation of the light-scattering properties of atmospheric aerosols was conducted from November 2015 to March 2017 at three functional sites in Nanjing. High concentrations of sulfate and nitrate in $PM_{0.56\text{-}1.0}$ were the major causes of the heavy particle pollution events. The varied abundance of secondary inorganic components at the three sites was an important reason for the visibility

differences, and OC played an important role on the visibility reduction in the industrial area due to its complicated optical effect. Based on the measured aerosol scattering coefficients and the mass concentrations of aerosol components, an optimized algorithm of IMPROVE that considered the light absorption effect of OM was developed to better represent the aerosol optical property.

Compared with internal and core-shell mixing states, the simulated scattering coefficients based on an external mixing assumption were closer to the measurements at NJU and PAES, indicating that externally mixed particles widely existed at urban and suburban areas. At the industrial site NUIST, the high aging level of SOA was the main reason for particle switching from external to internal mixing states. The results for the scattering coefficients under dry and ambient conditions indicated that RH had little effect on particle mixing state but a large impact on the scattering coefficients. Particles in the size range of 0.56-1.0 μm contributed the most (38%-63%) to the total scattering coefficient under different pollution levels. As the dominant light scattering species in aerosols, NH_4NO_3, $(NH_4)_2SO_4$ and OM collectively contributed 90%, 81% and 76% of the mass concentrations of $PM_{0.56\text{-}1.0}$ for the heavily polluted, lightly polluted and clean periods, respectively. The low visibility during the heavy pollution period mainly resulted from the enhanced light scattering of SNA. The abundance of light-absorption OC was an important reason for the relatively low contribution of OM to light scattering in the heavy pollution period.

Through a coupled model of PMF and Mie theory, we found coal combustion, industrial plants and vehicle were the main sources of the visibility reduction in Nanjing. Vehicles and industrial plants were the main causes for visibility reduction in urban and industrial areas, respectively. The increased emissions of SIA precursors from coal combustion were an important cause of polluted days, and the contribution of SOA to visibility reduction at industrial pollution areas should not be ignored. The source apportionment of aerosol light scattering in this work provides scientific evidence for the control of haze pollution in different functional areas of cities in developed eastern China.

DATA AVAILABILITY

All data in this study are available from the authors upon request.

AUTHOR CONTRIBUTIONS

DC developed the strategy and methodology of the work and wrote the draft. YZ improved the methodology and revised the manuscript. JZ, HY and XY provided observation data of aerosol scattering coefficient.

COMPETING INTERESTS

The authors declare that they have no conflict of interest.

ACKNOWLEDGEMENT

This work was sponsored by the Natural Science Foundation of China (41922052 and 91644220), and the National Key Research and Development Program of China (2017YFC0210106).

REFERENCES

Alexander, D. T. L., Crozier, P. A., Anderson, J. R.: Brown carbon spheres in East Asian outflow and their optical properties, Science, 321, 833-836, doi:10.1126/science.1155296, 2008.

Andreae, M. O., Schmid, O., Yang, H., Chand, D., Yu, J. Z., Zeng, L. M., Zhang, Y. H.: Optical properties and chemical composition of the atmospheric aerosol in urban Guangzhou, China, Atmos. Environ., 42, 6335-6350, doi:10.1016/j.atmosenv.2008.01.030, 2008.

Bohren, C. F, Huffman, D. R.: Absorption and scattering of light by small particles [R], New York: Wiley, Inc., 1998.

Bond, T. C., Bergstrom, R. W.: Light Absorption by Carbonaceous Particles: An

Investigative Review, Aerosol Sci. Technol., 40, 27-67, doi:10.1080/02786820500421521, 2006.

Cao, J. J., Lee, S. C., Chow, J. C., Watson, J. G., Ho, K. F., Zhang, R. J., Jin, Z. D., Shen, Z. X., Chen, G. C., Kang, Y. M., Zou, S. C., Zhang, L. Z., Qi, S. H., Dai, M. H., Cheng, Y., Hu, K.: Spatial and seasonal distributions of carbonaceous aerosols over China, J. Geophys. Res., 112, D22S11, doi:10.1029/2006JD008205, 2007.

Cao, J. J., Wang, Q. Y., Chow, J. C., Watson, J. G., Tie, X. X., Shen, Z. X., Wang, P., An, Z. S.: Impacts of aerosol compositions on visibility impairment in Xi'an, China, Atmos. Environ., 59, 559-566, doi:10.1016/j.atmosenv.2012.05.036, 2012.

Chen, D., Cui, H., Zhao, Y., Yin, L., Lu, Y., Wang, Q.: A two-year study of carbonaceous aerosols in ambient $PM_{2.5}$ at a regional background site for western Yangtze River Delta, China, Atmos. Res., 183, 351-361, doi:10.1016/j.atmosres.2016.09.004, 2017.

Chen, D., Zhao, Y., Lyu, R., Wu, R., Dai, L., Zhao, Y., Chen, F., Zhang, J., Yu, H., Guan, M.: Seasonal and spatial variations of optical properties of light absorbing carbon and its influencing factors in a typical polluted city in Yangtze River Delta, China, Atmos. Environ., 199, 45-54, doi:10.1016/j.atmosenv.2018.11.022, 2019.

Cheng, M. C., You, C. F., Cao, J., Jin, Z.: Spatial and seasonal variability of water soluble ions in PM2.5 aerosols in 14 major cities in China, Atmos. Environ., 60, 182-192, 10.1016/j.atmosenv.2012.06.037, 2012.

Cheng, S. H., Yang, L. X., Zhou, X. H., Xue, L. K., Gao, X. M., Zhou, Y., and Wang, W. X.: Size-fractionated water-soluble ions, situ pH and water content in aerosol on hazy days and the influences on visibility impairment in Jinan, China, Atmos. Environ., 45, 4631–4640, doi:10.1016/j.atmosenv.2011.05.057, 2011.

Cheng, Y., He, K.B., Du, Z.Y., Engling, G., Liu, J.M., Ma, Y.L., Zheng, M., Weber, R.J.: The characteristics of brown carbon aerosol during winter in Beijing, Atmos. Environ., 127, 355-364, doi:10.1016/j.atmosenv.2015.12.035, 2016.

Cheng, Y., He, K.B., Engling, G., Weber, R., Liu, J.M., Du, Z.Y., Dong, S.P.: Brown and black carbon in Beijing aerosol: Implications for the effects of brown coating on light absorption by black carbon, Sci. Total Environ., 599–600, 1047-1055.

doi:10.1016/j.scitotenv.2017.05.061, 2017.

Cheng, Z., Jiang, J., Chen, C., Gao, J., Wang, S., Watson, J.G., Wang, H., Deng, J., Wang, B., Zhou, M.: Estimation of aerosol mass scattering efficiencies under high mass loading: case study for the megacity of Shanghai, China, Environ. Sci. Technol., 49, 831-838, doi:10.1021/es504567q, 2015.

Cui, X., Wang, X., Yang, L., Chen, B., Chen, J., Andersson, A., Gustafsson, Ö.: Radiative absorption enhancement from coatings on black carbon aerosols, Sci. Total Environ., 551-552, 51-56, doi:10.1016/j.scitotenv.2016.02.026, 2016.

Ding, J., Han, S., Zhang, Y., Feng, Y., Wu, J., Shi, G., Wang, J.: Chemical characteristics of particles and light extinction effects in winter in Tianjin, Res. Environ. Sci., 28, 1353-1361, doi:10.13198/j.issn.1001-6929.2015.09.03, 2015.

Feng, J. L., Sun, P., Hu, X. L., Zhao, W., Wu, M. H., Fu, J. M.: The chemical composition and sources of PM2.5 during the 2009 Chinese New Year's holiday in Shanghai, Atmos. Res., 118, 435-444, doi:10.1016/j.atmosres.2012.08.012, 2012.

Huang, R. J., Yang, L., Cao, J., Chen, Y., Chen, Q., Li, Y., Duan, J., Zhu, C., Dai, W., Wang, K.: Brown Carbon Aerosol in Urban Xi'an, Northwest China: The Composition and Light Absorption Properties, Environ. Sci. Technol., 52, 6825-6833, doi:10.1021/acs.est.8b02386, 2018.

Huang, Y.W: Effects of changes in emission and meteorological conditions on fine particulate levels in the city scale, Master thesis, Nanjing University, 2018.

Hueglin, C., Gehrig, R., Baltensperger, U., Gysel, M., Monn, C., and Vonmont, H.: Chemical characterisation of PM2.5, PM10 and coarse particles at urban, near-city and rural sites in Switzerland, Atmos. Environ., 39, 637–651, doi:10.1016/j.atmosenv.2004.10.027, 2005.

Jacobson, M.Z.: Strong radiative heating due to the mixing state of black carbon in atmospheric aerosols, Nature, 409, 695-697, doi:10.1038/35055518, 2001.

Khan, M. F., Latif, M. T., Hwa, S. W., Amil, N., Nadzir, M. S. M., Sahani, M., Tahir, N. M., Jing, X. C.: Fine particulate matter in the tropical environment: monsoonal effects, source apportionment, and health risk assessment, Atmos. Chem. Phys., 16, 597-617, doi:10.5194/acp-16-597-2016, 2016.

删除的内容: .

980 Kim, E., Hopke, P.K.: Improving source identification of fine particles in a rural
981 northeastern US area utilizing temperature-resolved carbon fractions, J. Geophys.
982 Res.: Atmos., 109, D09204, doi:10.1029/2003jd004199, 2004.
983 Lai, S.C.: Characterization of PM2.5 and the major chemical components during a
984 1-year campaign in rural Guangzhou, Southern China, Atmos. Res., 167, 208-215,
985 doi:10.1016/j.atmosres.2015.08.007, 2016.
986 Lan, Z. J., Huang, X. F., Yu, K. Y., Sun, T. L., Zeng, L. W., Hu, M.: Light absorption
987 of black carbon aerosol and its enhancement by mixing state in an urban atmosphere
988 in South China, Atmos. Environ., 69, 118-123, doi:10.1016/j.atmosenv.2012.12.009,
989 2013.
990 Lang, J. L., Cheng, S. Y., Wen, W., Liu, C., Wang, G.: Development and application of
991 a new $PM_{2.5}$ source apportionment approach, Aerosol Air Qual. Res., 17, 340-350, doi:
992 10.4209/aaqr.2015.10.0588, 2017.
993 Lei, Y., Shen, Z., Wang, Q., Zhang, T., Cao, J., Sun, J., Zhang, Q., Wang, L., Xu, H.,
994 Tian, J., 2018. Optical characteristics and source apportionment of brown carbon in
995 winter PM2.5 over Yulin in Northern China, Atmos. Res., 213, 27-33,
996 doi:10.1016/j.atmosres.2018.05.018, 2018.
997 Li, B., Zhang, J., Zhao, Y., Yuan, S., Zhao, Q., Shen, G., Wu, H.: Seasonal variation of
998 urban carbonaceous aerosols in a typical city Nanjing in Yangtze River Delta, China,
999 Atmos. Environ., 106, 223-231, doi:10.1016/j.atmosenv.2015.01.064, 2015.
1000 Liu, X., Cheng, Y., Zhang, Y., Jung, J., Sugimoto, N., Chang, S. Y., Kim, Y. J., Fan, S.,
1001 Zeng, L.: Influences of relative humidity and particle chemical composition on
1002 aerosol scattering properties during the 2006 PRD campaign, Atmos. Environ., 42,
1003 1525-1536, doi:10.1016/j.atmosenv.2007.10.077, 2008.
1004 Liu, H. J., Zhao, C. S., Nekat, B., Ma, N., Herrmann, H.: Aerosol hygroscopicity
1005 derived from size-segregated chemical composition and its parameterization in the
1006 North China Plain, Atmos. Chem. Phys., 14, 2525-2539,
1007 doi:10.5194/acp-14-2525-2014, 2014.
1008 Liu, D., Whitehead, J., Alfarra, M. R., Reyesvillegas, E., Spracklen, D. V., Reddington,
1009 C. L., Kong, S., Williams, P. I., Ting, Y. C., Haslett, S.: Black-carbon absorption

enhancement in the atmosphere determined by particle mixing state, Nature Geosci., 10, 184-188, doi:10.1038/ngeo2901, 2017.

Lowenthal, D. H., Naresh, K.: PM2.5 mass and light extinction reconstruction in IMPROVE, J. Air Waste Manag. Assoc., 53, 1109-1120, doi:10.1080/10473289.2003.10466264, 2003.

Ma, N., Zhao, C. S., Müller, T., Cheng, Y. F., Liu, P. F., Deng, Z. Z., Xu, W. Y., Ran, L., Nekat, B., Van Pinxteren, D., Gnauk, T., Müller, K., Herrmann, H., Yan, P., Zhou, X.J., Wiedensohler, A.: A new method to determine the mixing state of light absorbing carbonaceous using the measured aerosol optical properties and number size distributions, Atmos. Chem. Phys., 12, 2381-2397, doi:10.5194/acp-12-2381-2012, 2012.

Malm, W.C., Hand, J. L.: An examination of the physical and optical properties of aerosols collected in the IMPROVE program, Atmos. Environ., 41, 3407-3427, doi:10.1016/j.atmosenv.2006.12.012, 2007.

Massabò, D., Caponi, L., Bove, M.C., Prati, P.: Brown carbon and thermal-optical analysis: A correction based on optical multi-wavelength apportionment of atmospheric aerosols, Atmos. Environ., 125, 119-125, doi:10.1016/j.atmosenv.2015.11.011, 2016.

Meier, J., Wehner, B., Massling, A., Birmili, W., Nowak, A., Gnauk, T., Bruggemann, E., Herrmann, H., Min, H., Wiedensohler, A.: Hygroscopic growth of urban aerosol particles in Beijing (China) during wintertime: a comparison of three experimental methods, Atmos. Chem. Phys., 9, 6865-6880, doi:10.5194/acp-9-6889-2009, 2009.

Ministry of Environmental Protection of China (MEP): Technical regulation on ambient air quality index, China Environ.Sci. Press, HJ633-2012, 2012.

Moon, K. J., Han, J. S., Ghim, Y. S., Kim, Y. J.: Source apportionment of fine carbonaceous particles by positive matrix factorization at Gosan background site in East Asia, Environ. Int., 34, 654-664, doi:10.1016/j.envint.2007.12.021, 2008.

Onasch, T. B., Massoli, P., Kebabian, P. L., Hills, F. B., Bacon, F. W., Freedman, A.: Single Scattering Albedo Monitor for Airborne Particulates, Aerosol Sci. Technol., 49, 267-279, doi:10.1080/02786826.2015.1022248, 2015.

带格式的: EndNote Bibliography, 行距: 1.5 倍行距

删除的内容: .

1041 Pakkanen, T. A., Kerminen, V. M., Hillamo, R. E., Makinen, M., Makela, T., and
1042 Virkkula, A.: Distribution of nitrate over seasalt and soil derived particles implications
1043 from a field study, J. Atmos. Chem., 24, 189–205, 1996.
1044 Petzold, A., Onasch, T., Kebabian, P., Freedman, A.: Intercomparison of a Cavity
1045 Attenuated Phase Shift-based extinction monitor (CAPS PMex) with an integrating
1046 nephelometer and a filter-based absorption monitor, Atmos. Meas. Tech., 6,
1047 1141-1151, doi:10.5194/amt-6-1141-2013, 2013.
1048 Pitchford, M., Malm, W., Schichtel, B., Kumar, N., Lowenthal, D., Hand, J.: Revised
1049 algorithm for estimating light extinction from IMPROVE particle speciation data, J.
1050 Air Waste Manag. Assoc., 57, 1326-1336, doi:10.3155/1047-3289.57.11.1326, 2007.
1051 Ramanathan, V., Li, F., Ramana, M. V., Praveen, P. S., Kim, D., Corrigan, C. E.,
1052 Nguyen, H., Stone, E. A., Schauer, J. J., Carmichael, G. R., Adhikary, B., Yoon, S. C.:
1053 Atmospheric brown clouds: Hemispherical and regional variations in long-range
1054 transport, absorption, and radiative forcing, J. Geophys. Res.: Atmos., 112, D22S21,
1055 doi:10.1029/2006JD008124, 2007.
1056 Schwartz, S.: The Whitehouse Effect–Shortwave radiative forcing of climate by
1057 anthropogenic aerosols: An overview, J. Aerosol Sci., 27, 359–382,
1058 doi:10.1016/0021-8502(95)00533-1, 1996.
1059 Seinfeld, J. H., Pandis.: Atmospheric chemistry and physics: From air pollution to
1060 climate change, doi:10.1080/00139157.1999.10544295, 2006.
1061 Shao, P., An, J., Xin, J., Wu, F., Wang, J., J, D., Wang, Y.: Source apportionment of
1062 VOCs and the contribution to photochemical ozone formation during summer in the
1063 typical industrial area in the Yangtze River Delta, China, Atmos. Res., 176-177, 64-74,
1064 doi:10.1016/j.atmosres.2016.02.015, 2016.
1065 Shi, Y., Chen, J., Hu, D., Wang, L., Yang, X., Wang, X.: Airborne submicron
1066 particulate (PM1) pollution in Shanghai, China: chemical variability,
1067 formation/dissociation of associated semi-volatile components and the impacts on
1068 visibility, Sci. Total Environ., 473, 199-206, 10.1016/j.scitotenv.2013.12.024, 2014.
1069 Swietlicki, E., Hansson, H. C., Hämeri, K., Svenningsson, B., Massling, A.,
1070 McFiggans, G., McMurry, P. H., Petäjä, T., Tunved, P., Gysel, M., Topping, D.,

Weingartner, E., Baltensperger, U., Rissler, J., Wiedensohler, A., Kulmala, M.: Hygroscopic properties of submicrometer atmospheric aerosol particles measured with H-TDMA instruments in various environments – a review, Tellus B, 60, 432–469, doi:10.1111/j.1600-0889.2008.00350.x, 2008.

Tang, I. N.: Chemical and size effects of hygroscopic aerosols on light scattering coefficients, J. Geophys. Res.: Atmos., 101, 19245-19250, doi:10.1029/96jd03003, 1996.

Tao, J., Cheng, T., Zhang R.: Chemical composition of PM2.5 at an urban site of Chengdu in southwestern China, Adv. Atmos. Sci., 30, 1070-1084, doi:10.1007/s00376-012-2168-7, 2013.

Tao, J. C , Zhao, C. S., Ma, N., Liu, P. F.: The impact of aerosol hygroscopic growth on the single-scattering albedo and its application on the NO_2 photolysis rate coefficient, Atmos. Chem. Phys., 14, 12055-12067, doi:10.5194/acp-14-12055-2014, 2014a.

Tao, J., Zhang, L., Cao, J., Hsu, S. C., Xia, X., Zhang, Z., Lin, Z., Cheng, T., Zhang, R.: Characterization and source apportionment of aerosol light extinction in Chengdu, southwest China, Atmos. Environ., 95, 552-562, doi:10.1016/j.atmosenv.2014.07.017, 2014b.

Tao, J., Zhang, L., Kinfai, H. O., Zhang, R., Lin, Z., Zhang, Z., Lin, M., Cao, J., Liu, S., Wang, G.: Impact of $PM_{2.5}$ chemical compositions on aerosol light scattering in Guangzhou - the largest megacity in South China, Atmos. Res., 135-136, 48-58, doi:10.1016/j.atmosres.2013.08.015, 2014c.

Tao. J., Zhang, L., Gao. J., Wang. H., Chai. F., Wang. S: Aerosol chemical composition and light scattering during a winter season in Beijing, Atmos. Environ., 110, 36-44, doi:10.1016/j.atmosenv.2015.03.037, 2015.

Tian, S. L., Pan, Y. P., Liu, Z., Wen, T., and Wang, Y. S.: Size-resolved aerosol chemical analysis of extreme haze pollution events during early 2013 in urban Beijing, China, J. Hazard. Mater., 279, 452–460, doi:10.1016/j.jhazmat.2014.07.023, 2014.

Tian, S. L., Pan, Y. P., Wang, Y. S.: Size-resolved source apportionment of particulate matter in urban Beijing during haze and non-haze episodes, Atmos. Chem. Phys., 16,

删除的内容: Tian, S. L., Pan, Y. P., Wang, Y. S.: Size-resolved source apportionment of particulate matter in urban Beijing during haze and non-haze episodes, Atmos. Chem. Phys., 15, 9405-9443, doi:10.5194/acp-15-9405-2015, 2015. .

1-19, doi:10.5194/acp-16-1-2016, 2016.

Titos, G., Cazorla, A., Zieger, P., Andrews, E., Lyamani, H., Granados-Muñoz, M. J., Olmo, F. J., Alados-Arboledas, L.: Effect of hygroscopic growth on the aerosol light-scattering coefficient: A review of measurements, techniques and error sources, Atmos. Environ., 141, 494-507, doi:10.1016/j.atmosenv.2016.07.021, 2016.

Wang, H., An, J., Cheng, M., Shen, L., Zhu, B., Li, Y., Wang, Y., Duan, Q., Sullivan, A., Xia, L.: One year online measurements of water-soluble ions at the industrially polluted town of Nanjing, China: Sources, seasonal and diurnal variations, Chemosphere, 148, 526-536, doi:10.1016/j.chemosphere.2016.01.066, 2016a.

Wang. J., Zhang, Y., Feng, Y., Zheng, X., Li, J., Hong, S., Shen, J., Tan, Z., Jing, D., Qi, Z.: Characterization and source apportionment of aerosol light extinction with a coupled model of CMB-IMPROVE in Hangzhou, Yangtze River Delta of China, Atmos. Res., 178-179, 570-579, doi:10.1016/j.atmosres.2016.05.009, 2016b.

Wang, S. R., Yu, Y. Y., Wang, Q. G., Lu, Y., Yin, L. N., Zhang, Y. Y., Lu, X. B.: Source apportionment of $PM_{2.5}$ in Nanjing by PMF, China Environ.Sci., 35, 3535-3542, 2015.

Watson, J. G.: Visibility: Science and regulation, J. Air Waste Manage. Assoc., 52, 628-713, 2002.

Watson, J. G., Chow, J. C., Lowenthal, D. H., L-W, A. C., Stephanie, S., Edgerton, E. S., Blanchard, C. L.: $PM_{2.5}$ source apportionment with organic markers in the Southeastern Aerosol Research and Characterization (SEARCH) study, J. Air Waste Manage. Assoc., 65, 1104-1118, doi:10.1080/10962247.2015.1063551, 2015.

Xu, J., Bergin, M. H., Yu, X., Liu, G., Zhao, J., Carrico, C. M., Baumann, K.: Measurement of aerosol chemical, physical and radiative properties in the Yangtze delta region of China, Atmos. Environ., 36, 161-173, doi:10.1016/s1352-2310(01)00455-1, 2002.

Xu, J., Tao, J., Zhang, R., Cheng, T., Leng, C., Chen, J., Huang, G., Li, X., Zhu, Z.: Measurements of surface aerosol optical properties in winter of Shanghai, Atmos. Res., 109-110, 25-35, doi:10.1016/j.atmosres.2012.02.008, 2012.

Xue, L., Ding, A., Gao, J., Wang, T., Wang, W., Wang, X., Lei, H., Jin, D., Qi, Y.: Aircraft measurements of the vertical distribution of sulfur dioxide and aerosol

scattering coefficient in China, Atmos. Environ., 44, 278-282, doi:10.1016/j.atmosenv.2009.10.026, 2010.

Yan, C. Q., Zheng, M., Zhang, Y. H.: Research progress and direction of atmospheric brown carbon, Environ. Sci., 35, 4404-4414, doi:10.13227/j.hjkx.2014.11.050, 2014.

Yang, F., Tan, J., Zhao, Q., Du, Z., He, K., Ma, Y., Duan, F., Chen, G., Zhao, Q.: Characteristics of $PM_{2.5}$ speciation in representative megacities and across China, Atmos. Chem. Phys., 11, 5207-5219, doi:10.5194/acp-11-5207-201, 2011.

Zhang, L., Sun, J. Y., Shen, X. J., Zhang, Y. M., Che, H. C., Ma, Q. L., Zhang, Y. W., Zhang, X. Y., Ogren, J. A.: Observations of relative humidity effects on aerosol light scattering in the Yangtze River Delta of China, Atmos. Chem. Phys., 15, 2853-2904, doi:10.5194/acp-15-8439-2015, 2015.

Zhang, Y., Forrister, H., Liu, J., Dibb, J., Anderson, B., Schwarz, J. P., Perring, A. E., Jimenez, J. L., Campuzanojost, P., Wang, Y.: Top-of-atmosphere radiative forcing affected by brown carbon in the upper troposphere, Nature Geosci., 10, doi:10.1038/ngeo2960, 2017.

Zhao, P. S., Dong, F., He, D., Zhao, X. J., Zhang, W. Z., Yao, Q., Liu, H. Y.: Characteristics of concentrations and chemical compositions for PM2.5 in the region of Beijing, Tianjin, and Hebei, China, Atmos. Chem. Phys., 13, 4631-4644. doi:10.5194/acp-13-4631-2013, 2013.

Zhao, Y., Qiu, L. P., Xu, R., Xie, F., Zhang, Q., Y. Yu, Y., Nielsen, C. P., Qin, H., Wang, H., Wu, X., Q. Li, W., Zhang, J.: Advantages of a city-scale emission inventory for urban air quality research and policy: the case of Nanjing, a typical industrial city in the Yangtze River Delta, China, Atmos. Chem. Phys., 15, 12623-12644. doi:10.5194/acpd-15-18691-2015, 2015.

FIGURE CAPTIONS

Figure 1. The mass concentrations and fractions of the main chemical components of particles with different sizes in Nanjing on clean, lightly-polluted and heavily-polluted days during the sampling period.

Figure 2. Linear regressions between the measured light scattering coefficients and those estimated with the optimized IMPROVE algorithm at NJU, PAES, NUIST and all three sites.

Figure 3. The comparison of measured and estimated dry scattering coefficients based on the assumptions of external, internal, and core-shell mixture at NJU (a), PAES (b) and NUIST (c).

Figure 4. The size distribution of hygroscopic scattering growth of particles under varied relative humidity levels at the three sites.

Figure 5. The size distribution of scattering coefficients of aerosol particles (a), $(NH_4)_2SO_4$ (b), NH_4NO_3 (c) and OM (d) under different pollution levels. The contributions of particles with different sizes to total scattering coefficient are indicated in the panels as well.

Figure 6. The size distribution of mass concentrations of $(NH_4)_2SO_4$, NH_4NO_3 (a), and OM (b) under different pollution levels and mass scattering efficiencies (MSE) for $PM_{1.8}$. The size of dot represents the MSEs of $PM_{1.8}$ (Unit: m^2/g).

Figure 7. Source apportionment of accumulation mode particles at NJU (a), PAES (b) and NUIST (c), and source apportionment of light scattering for accumulation mode particles at NJU (d), PAES (e) and NUIST (f). The shadow represents the contribution of secondary aerosols from each source category.

Figure 8. Source apportionment of light scattering for accumulation mode particles for the clean and polluted periods at NJU (a), PAES (b) and NUIST (c). The shadow represents the contribution of secondary aerosols from each source category.

TABLES

Table 1. The concentrations of particulate matter and its chemical components (μg/m^3), light scattering coefficients (Mm^{-1}), and selected meteorological parameters including wind speed (WS, m/s) and relative humidity (RH, %) at all the three sites for different pollution levels from November 2015 to January 2017.

Category	Clean period	Lightly polluted period	Heavily polluted period
AQI	65.8 ± 15.7	110.6 ± 21.3	209.4 ± 30.1
PM_{10}	80.4 ± 26.3	143.1 ± 28.6	244.2 ± 21.2
$PM_{2.5}$	47.9 ± 15.8	102.1 ± 16.4	163.1 ± 13.6
OC	8.6 ± 3.2	14.2 ± 3.2	27.6 ± 5.0
EC	1.9 ± 0.9	3.0 ± 1.2	5.3 ± 0.1
SO_4^{2-}	6.9 ± 3.9	13.5 ± 5.6	33.8 ± 9.2
NO_3^-	10.5 ± 5.4	22.7 ± 8.7	47.9 ± 17.7
Cl^-	1.8 ± 1.5	2.2 ± 1.3	4.8 ± 1.4
Ca^{2+}	1.2 ± 0.8	1.3 ± 1.6	0.8 ± 0.1
Na^+	0.8 ± 0.2	0.9 ± 0.3	1.0 ± 0.1
Mg^{2+}	0.1 ± 0.1	0.2 ± 0.1	0.1 ± 0.0
NH_4^+	5.1 ± 1.9	9.2 ± 2.2	16.9 ± 2.5
K^+	0.9 ± 0.2	1.3 ± 0.3	2.1 ± 0.7
CO	0.8 ± 0.2	1.3 ± 0.3	1.6 ± 0.1
NO_2	57.4 ± 18.0	71.6 ± 20.0	91.2 ± 32.8
SO_2	17.7 ± 6.5	21.1 ± 6.0	29.5 ± 12.5
WS	1.6 ± 0.3	1.4 ± 0.5	1.0 ± 0.3
RH	56.1 ±13.5	62.7 ± 10.8	68.9 ± 4.9
b_{sp}	251.4 ± 170.8	558.3 ± 236.4	1286.2 ± 293.3

Table 2. The mass scattering efficiencies (MSEs, m^2/g) of chemical species in the optimized and the existing algorithms from the Interagency Monitoring of Protected Visual Environments (IMPROVE). The sample numbers and the mass fractions of light-absorption BrC to MSOC for small and large size modes (i.e., *m* and *n* in Eq.1) are provided for the optimized algorithm.

	Modes	NJU	PAES	NUIST	All the three sites	IMPROVE 2007	IMPROVE 1999
MSE of $(NH_4)_2SO_4$	small	2.32	2.02	2.43	2.29	2.2	-
	large	4.71	4.92	4.86	4.82	4.8	-
	overall	3.91	3.88	4.03	3.94	-	3
MSE for NH_4NO_3	small	2.67	2.48	2.56	2.62	2.4	-
	large	5.37	5.31	5.26	5.35	5.1	-
	overall	4.41	4.13	4.23	4.31	-	3
MSE of OM	small	4.4	4.56	4.22	4.46	2.8	-
	large	6.23	6.36	6.45	6.41	6.1	-
	overall	5.26	5.03	5.35	5.25	-	4
m	-	0.66	0.71	0.39	0.67	-	-
n	-	0.29	0.27	0.33	0.31	-	-
Sample number	-	174	45	63	282	-	-

Table 3. The source contributions of secondary aerosols to aerosol light scattering at the three sites for the clean and polluted periods (%).

Air quality level	Sources	NJU		PAES		NUIST	
		SIA	SOA	SIA	SOA	SIA	SOA
Clean	Coal combustion	6.6	0.8	6.5	1.1	7.5	1.3
	Industrial plants	5.8	3.6	4.2	1.5	8.2	6.3
	Vehicles	2.1	1.0	6.1	1.5	4.2	1.1
	Total	19.9		20.9		28.6	
Polluted	Coal combustion	12.4	1.6	8.8	2.3	10.2	2.2
	Industrial plants	10.2	5.8	7.8	3	12.6	9.9
	Vehicles	5.0	1.7	7.9	2.6	5.2	1.6
	Total	36.7		32.4		41.7	

Figure 1

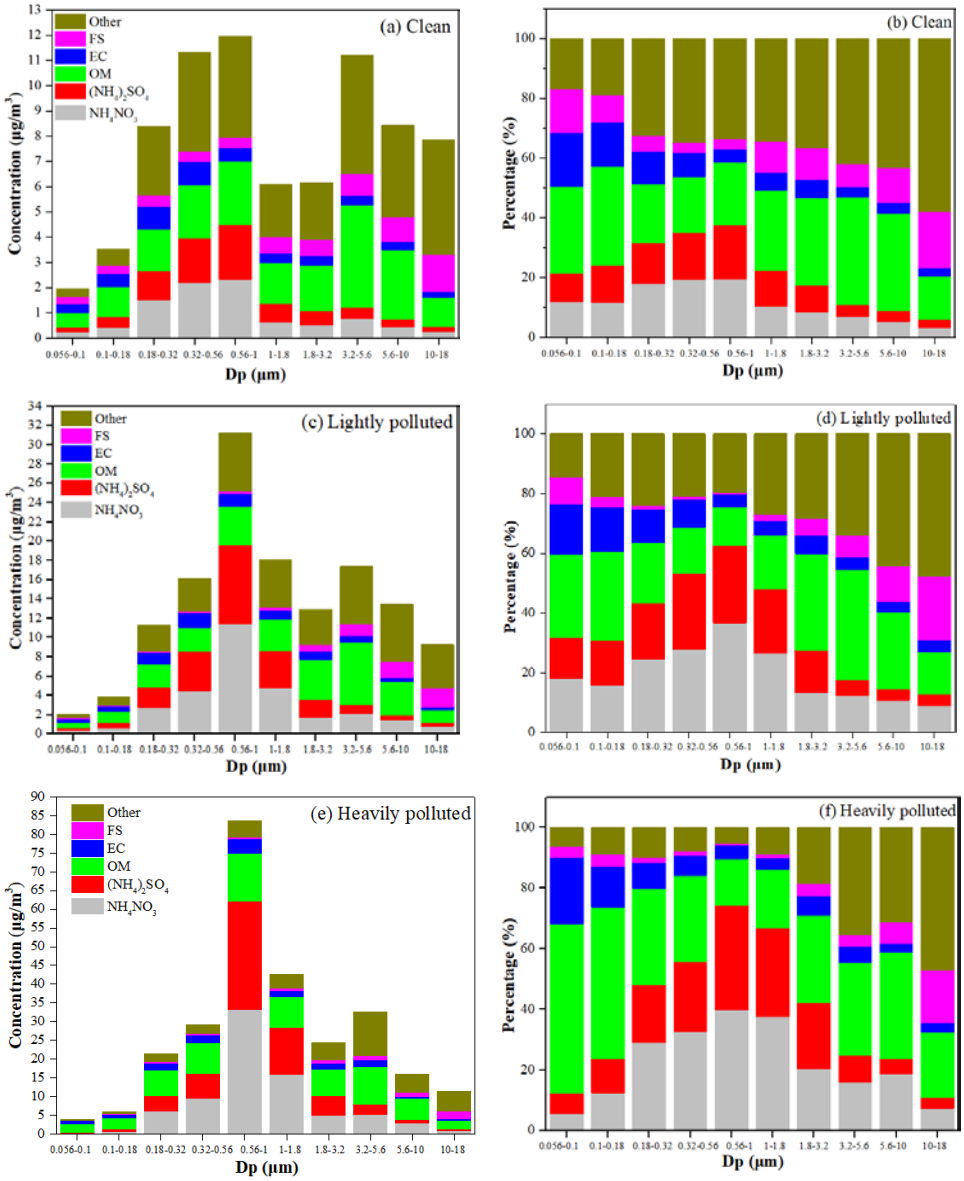
(a) Clean
(b) Clean
(c) Lightly polluted
(d) Lightly polluted
(e) Heavily polluted
(f) Heavily polluted
Other
FS
EC
OM
(NH4)2SO4
NH4NO3
Concentration (μg/m3)
Percentage (%)
Dp (μm)
0.056-0.1
0.1-0.18
0.18-0.32
0.32-0.56
0.56-1
1-1.8
1.8-3.2
3.2-5.6
5.6-10
10-18

Figure 2

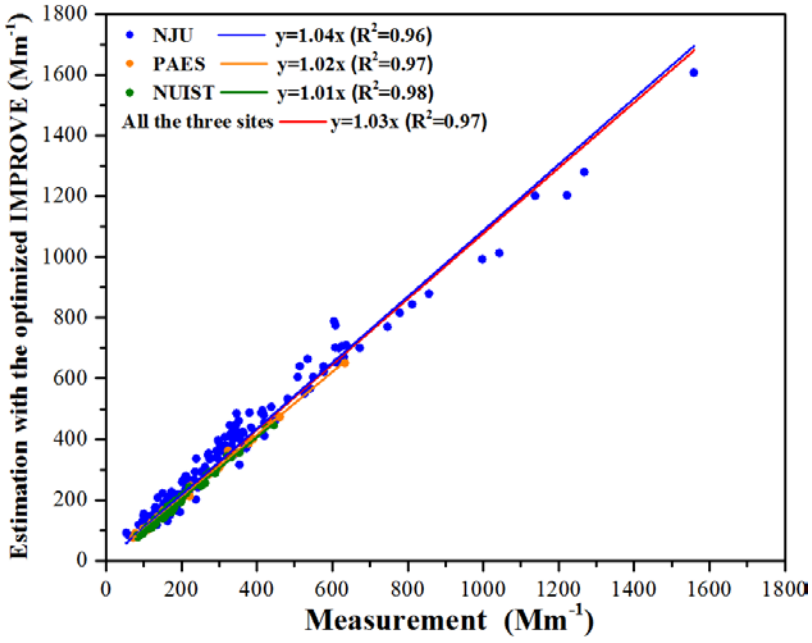
NJU y=1.04x (R²=0.96)
PAES y=1.02x (R²=0.97)
NUIST y=1.01x (R²=0.98)
All the three sites y=1.03x (R²=0.97)
Estimation with the optimized IMPROVE (Mm⁻¹)
Measurement (Mm⁻¹)
0
200
400
600
800
1000
1200
1400
1600
1800

1214

1215 **Figure 3**

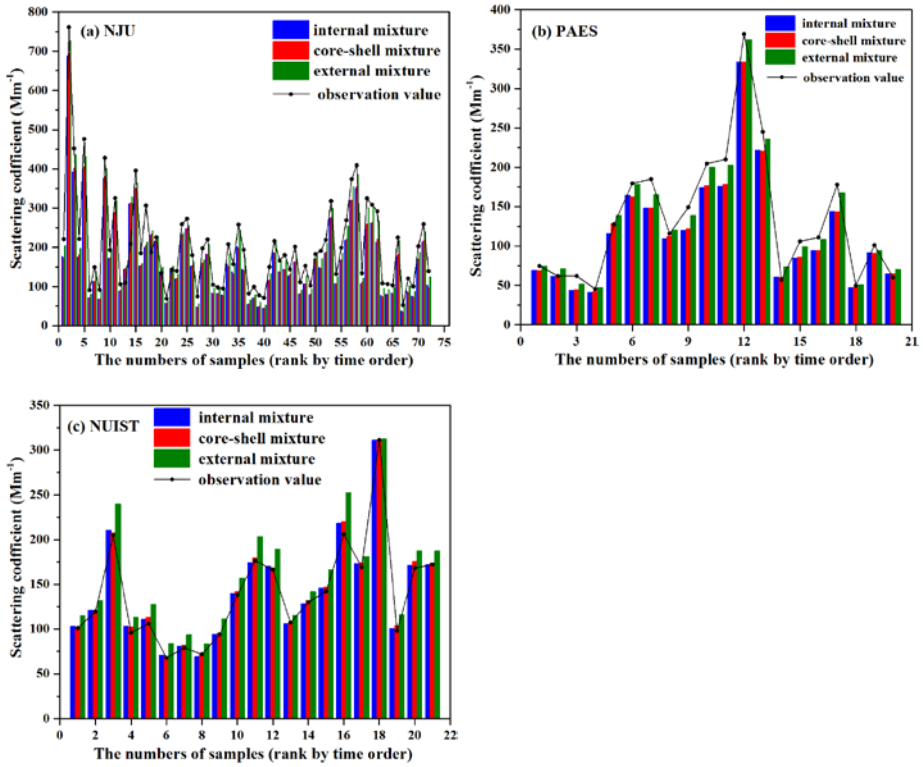

1216

Figure 4

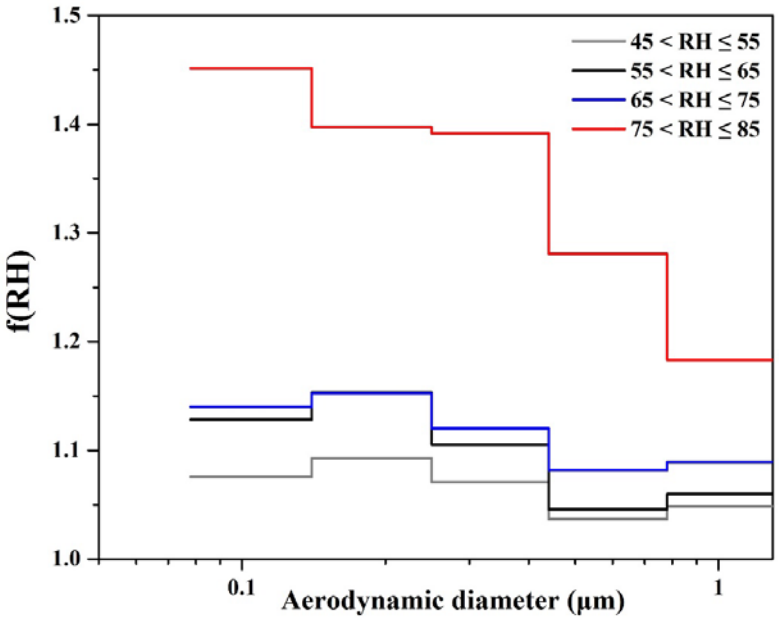
45 < RH ≤ 55
55 < RH ≤ 65
65 < RH ≤ 75
75 < RH ≤ 85
f(RH)
1.5
1.4
1.3
1.2
1.1
1.0
0.1
1
Aerodynamic diameter (μm)

1221

1222 **Figure 5**

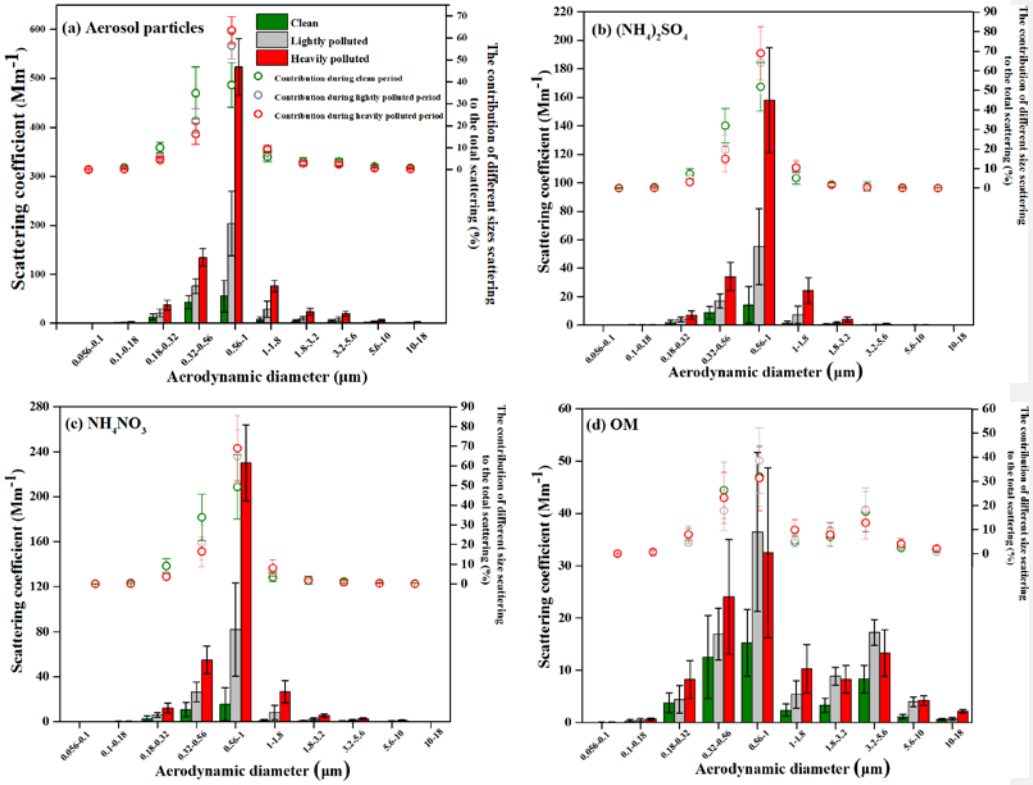

1223

1224

1225 **Figure 6**

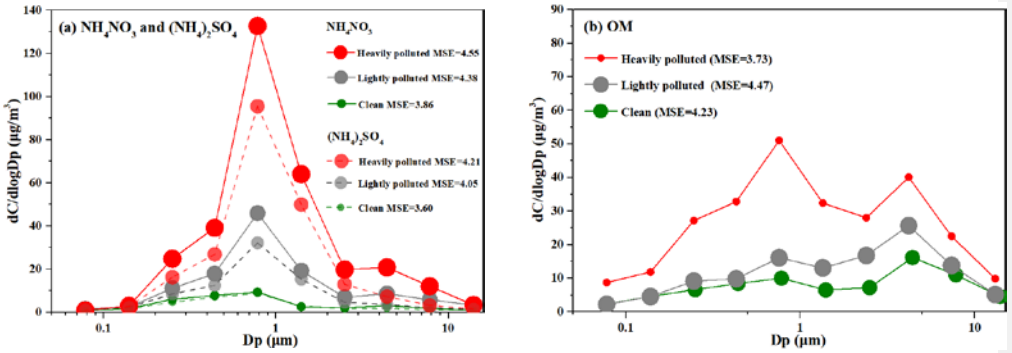

1226

1227

1228 **Figure 7**

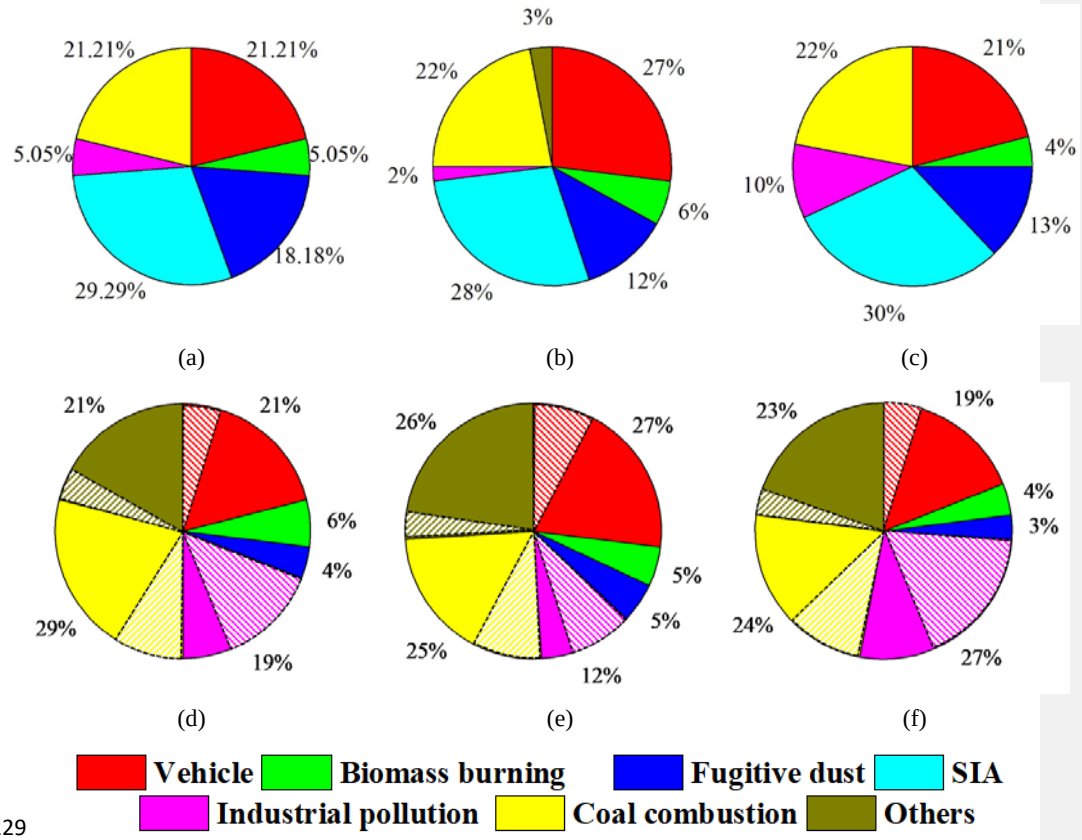

1229

Figure 8

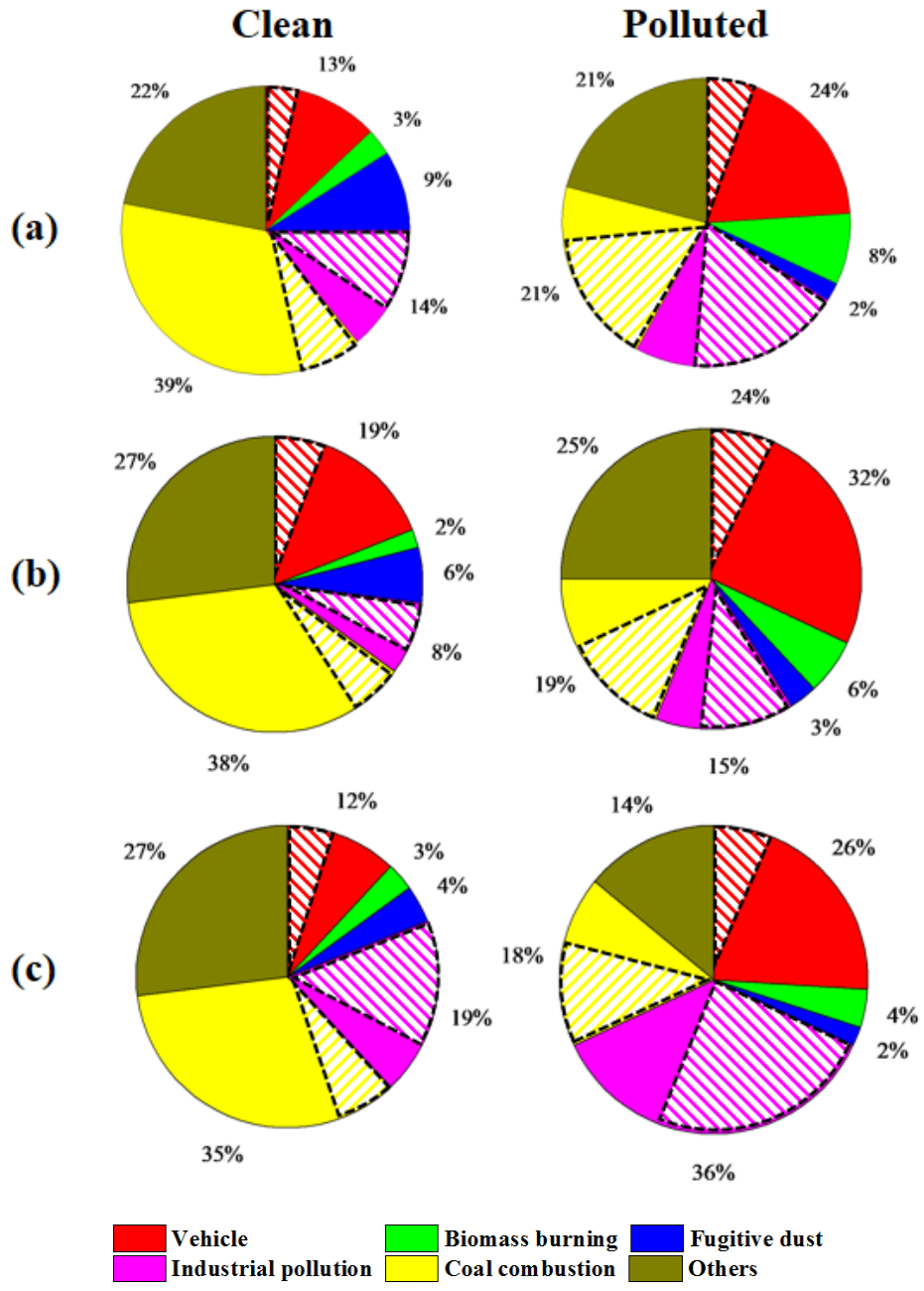
Clean
Polluted
(a)
(b)
(c)
13%
3%
9%
14%
39%
22%
21%
24%
8%
2%
24%
21%
19%
2%
6%
8%
38%
27%
25%
32%
6%
3%
15%
19%
12%
3%
4%
19%
35%
27%
14%
26%
4%
2%
36%
18%
Vehicle
Industrial pollution
Biomass burning
Coal combustion
Fugitive dust
Others